Clim. Past Discuss., 7, 3349–3397, 2011
www.clim-past-discuss.net/7/3349/2011/
doi:10.5194/cpd-7-3349-2011
© Author(s) 2011. CC Attribution 3.0 License.

Climate of the Past Discussions

This discussion paper is/has been under review for the journal Climate of the Past (CP).
Please refer to the corresponding final paper in CP if available.

Northern Hemisphere temperature patterns in the last 12 centuries

F. C. Ljungqvist[1,2], P. J. Krusic[3,4], G. Brattström[5], and H. S. Sundqvist[3,4]

[1]Department of History, Stockholm University, 106 91 Stockholm, Sweden
[2]Centre for Medieval Studies, Stockholm University, 106 91 Stockholm, Sweden
[3]Bert Bolin Centre for Climate Research, Stockholm University, 106 91 Stockholm, Sweden
[4]Department of Physical Geography and Quaternary Geology, Stockholm University, 106 91 Stockholm, Sweden
[5]Department of Mathematics, Stockholm University, 106 91 Stockholm, Sweden

Received: 30 September 2011 – Accepted: 5 October 2011 – Published: 13 October 2011

Correspondence to: F. C. Ljungqvist (fredrik.c.l@historia.su.se)

Published by Copernicus Publications on behalf of the European Geosciences Union.

Abstract

We analyze the spatio-temporal patterns of temperature variability over Northern Hemisphere land areas, on centennial time-scales, for the last 12 centuries using an unprecedentedly large network of temperature-sensitive proxy records. Geographically widespread positive temperature anomalies are observed from the 9th to 11th centuries, similar in extent and magnitude to the 20th century mean. A dominance of widespread negative anomalies is observed from the 16th to 18th centuries. Though we find the amplitude and spatial extent of the 20th century warming is within the range of natural variability over the last 12 centuries, we also find that the rate of warming from the 19th to the 20th century is unprecedented. The positive Northern Hemisphere temperature change from the 19th to the 20th century is clearly the largest between any two consecutive centuries in the past 12 centuries.

1 Introduction

A number of Northern Hemispheric (NH) temperature reconstructions covering the last 1–2 millennia, using temperature-sensitive proxy data, have been made to place the observed 20th century warming into a long-term perspective (Briffa, 2000; Christiansen and Ljungqvist, 2011; Cook et al., 2004; Crowley and Lowery, 2000; D'Arrigo, 2006; Esper et al., 2002; Hegerl et al., 2007; Jones et al., 1998; Jones and Mann, 2004; Juckes et al., 2007; Ljungqvist, 2008; Mann et al., 1999, 2008, 2009; Mann and Jones, 2003; Moberg et al., 2005; Osborn and Briffa, 2006). These studies generally agree on the occurrence of warmer conditions 800–1300 c. AD and colder conditions 1300–1900 c. AD, followed by a strong warming trend in the 20th century (Jansen et al., 2007). The earlier warm period is usually referred to as the Medieval Warm Period (MWP) or Medieval Climate Anomaly (MCA) (Bradley et al., 2003; Broecker, 2001; Diaz et al., 2011; Esper and Frank, 2009; Hughes and Diaz, 1994) whereas the later colder period is often referred to as the Little Ice Age (LIA) (Grove, 1988; Juckes et

CPD
7, 3349–3397, 2011

al., 2007; Matthews and Briffa, 2005; National Research Council, 2006; Wanner et al., 2008, 2011). Related to this issue is the question of whether or not the current warmth has exceeded the level and geographic extent of the warmth in the last millennium.

Placing the level of the recent warming in context to past warmth does not alone tell us anything about the physical processes responsible for either. Yet, having the ability to distinguish, on a hemispheric-scale, between a homogeneous and a heterogeneous climate state is fundamental to our understanding of plausible climate forcings. It has been suggested that only large-scale climate averages reflect a response to global forcings (Jansen et al., 2007) and recent studies of reconstructed global temperature patterns imply a dynamic response of climate variability due to natural radiative forcing are detectable (Mann et al., 2009). At the same time, it has been noted that the use of too few noisy and poorly replicated proxies precludes a satisfactory assessment of spatial temperature anomalies, particularly in medieval times, the nearest analogue to the present (Esper and Frank, 2009; Broecker, 2001). Therefore, it is essential to refine our knowledge of the temporal evolution of spatial climate variability. We suggest this cannot be satisfactorily done without considering all the available proxy evidence.

Previous hemispheric-scale, temperature reconstructions over the past millennium, with one notable exception (Mann et al., 2009), have focused on reconstructing temperatures in the time domain only, an understandable consequence resulting from few and sparsely distributed high-resolution proxies that can be calibrated directly against instrumental observations. The unique approach of Mann et al. (2009) attempts to overcome this problem by taking advantage of statistically determined spatial teleconnections between instrumental temperature fields and temperature, precipitation or drought sensitive proxy data as well. An example is the strong correlation between the moisture-sensitive tree-ring series in the American Southwest and sea surface temperatures in the tropical Pacific ENSO region (Wilson et al., 2010). This approach relies heavily on the assumption that both the spatial and temporal relationships found between the modern (proxy vs. climate) measurements have remained constant through time and that these relationships are linear. Nevertheless, due to the method, the

CPD
7, 3349–3397, 2011

Mann et al. (2009) reconstructed medieval period is still based on relatively few, spatially well distributed, proxies. Arguably, a substantially denser proxy network should produce a more robust reconstruction. This can be done if one accepts proxies with lower temporal resolution and if the proxies used are constrained to be indicators of local temperature. However, the decision to include low-resolution proxies results in the loss of temporal detail (resolution) and the inability to produce a temperature calibrated reconstruction. We suggest these drawbacks are not detrimental to the exercise and in fact permit accurate descriptions of climate variability in both time and space on centennial time-scales.

2 Proxy data and method

Here we present a new reconstruction of the spatio-temporal patterns of centennial temperature variability over the NH land areas for the last twelve centuries based on 120 proxy records (Fig. 1; Table A1). An extensive search of the literature for proxy records possessing annual to sub-centennial resolution covering at least the last millennium, and considered by their authors to be temperature sensitive, was conducted. The proxies are retrieved from a wide range of archives including, but not limited to, ice-cores, pollen, marine sediments, lake sediments, tree-rings, speleothems and historical documentary data (Table A1). We concede that each proxy type has its inherent strengths and weaknesses as a palaeo-thermometer. Numerous books and articles describe the use and interpretation of the proxy types used in this experiment. Therefore, we forego a lengthy discussion on climate proxies here and instead refer the reader to Bradley (1999) and Jones et al. (2009), and the references within, for a comprehensive overview of palaeoclimatology.

The data are also diverse not only in their type, resolution and location but also in the temperature signal they are reported to contain. Most high-latitude proxies primarily record summer temperatures while most low-latitude proxies primarily record

CPD
7, 3349–3397, 2011

annual mean temperatures. The mid-latitude proxies may have either a summer or annual mean temperature signal. Only eight of the proxies used are purported to be expressions of winter temperature.

To obtain a network of widely distributed temperature proxies we accepted records having as few as two data points per century. The decision to use low-resolution proxy data confines our analyses to no less than centennial variations but delivers substantially larger spatial coverage, particularly, prior to 1400 c. AD. Since many of the proxies used cannot be reliably calibrated into temperatures we use centennial anomalies normalized with respect to the 11th–19th centuries. This is the period fully covered by all 120 proxies. For proxies sampled at time steps greater than one year a linear interpolation was applied to produce an annually resolved time-series that can be smoothed with a 167-year spline. Every 25th annual spline value, from 800 AD to 1950 AD, forms a new time series of 45 centennial means. The 45 centennial means from each proxy record is normalized by its mean and standard deviation over the 11th to 19th centuries (1000 AD to 1899 AD) (Fig. 4). The twelve normalized centennial anomalies, located in the middle of each whole century (e.g. 800 AD, 900 AD, 1000 AD ..., 1900 AD), are used for the spatial comparisons in Figs. 2–3. See Appendix A for more details.

The spatial-temporal evolution of anomalies is dynamically displayed in an 1101-year animation from 850 AD to 1950 AD. At every proxy location an Akima spline is fit to each proxy's 45 centennial mean values (raw and weighted) producing a smooth, centennial trend, interpolation with a time step of one year. The four animations produced, available as an electronic Supplement are, (i) the filtered spline values, (ii) the gridded, filtered spline values, (iii) the proxy-centered, weighted mean, filtered spline values, and (iv) the gridded, proxy-centered, weighted mean, filtered spline values. The first purpose of this exercise is to demonstrate how the weighted mean and gridding algorithms affect the transformation of the raw data. The Akima spline is very efficient in handling discontinuous time series data to produce continuous interpolations without inducing spurious wiggles because no parametric curve form is assumed and only the local data nodes are taken into account (Akima, 1970). Secondly, producing these

CPD
7, 3349–3397, 2011

1101 slices of the spatial field permits one to examine the temporal stability of both proxy-local, and proxy extra-local patterns produced by the analysis.

2.1 Weighted anisotropic averaging and gridding

The real spatial variability of centennial mean temperatures is certainly more coherent than the centennial mean anomalies show in Fig. 2. We infer from Jones et al. (1997) that the global-mean correlation decay length, for unforced centennial temperature variability, is at least ~2000 km and decreases from low to high latitudes. The correlation decay length is the distance at which spatial temperature correlations between meteorological stations, on average, falls to ≈0.37 (see Appendix A for more details). Due to the diversity of proxies used it is more relevant to look into how groups of neighbouring proxies behave than to focus on any individual record. This approach is not that dissimilar to the approach taken in the evaluation of Global Circulation Models by using their ensemble means.

To obtain a clearer view of the spatial patterns of temperature variability provided by the proxies we first applied a weighted averaging to the centennial anomalies, centred over each proxy location, for all 45 centennial means. A Gaussian weight function that decreases from 1, at the proxy node, to $e^{-2} \approx 0.14$ at the search periphery was used to compute a weighted mean. Proxy centred, weighted mean, centennial values are computed only if a proxy has two or more neighbours with data for the same century and those neighbours lie within a meridionally defined, anisotropic, search radius that decreases from 2000 km at the equator to 1000 km at the North Pole. Gridding of these spatially weighted, proxy-centred, centennial means was performed using a modified nearest neighbour gridding algorithm that requires at least 3 proxies within the search radius of each node of a $1^\circ \times 1^\circ$ Cartesian grid. The weighted mean grid value was calculated from the weighted-mean centennial proxy values using the same Gaussian weight and anisotropic search functions described above. Though the oceans have been masked on the maps, coastal marine proxy records may contribute to the land area grid (see Appendix A for more details). The gridding procedure smoothes

CPD
7, 3349–3397, 2011

small-scale variations as seen in the individual proxies (in Fig. 2) and retains only those variations that are spatially distinct (Fig. 3).

2.2 Test of robustness

To test the robustness of the proxy data used and the observed spatial patterns they produce we undertook a number of experiments, like the one shown in Fig. 3, using different subsets of the proxies. The results from these experiments are provided in the accompanying supplement to this article. The five different experiments were performed are: (i) excluding one proxy data type at a time (ii) using only those proxies that begin before 816 AD and end after 1984 AD (iii) using only proxies with 4 or more, and also with 10 or more, observations per century (iv) requiring that each proxy series used must have data coverage up to 1995 and (v) excluding the 43 proxy series that have either a negative correlation to the mean time-series of their proxy centred, within-search-radius, neighbours or less than two within-search-distance neighbours. No result from of these five experiments significantly changes our main observations regarding the spatio-temporal patterns of past temperature variability. The results of these experiments are only shown in the Supplement to this article in Figs. S1–S13 with supporting text.

3 Results

The spatial and temporal patterns of centennial temperature proxy anomaly values at each proxy location, for the last twelve centuries, are illustrated in Fig. 2. In addition to the large-scale patterns that clearly emerge (a dominance of warm anomalies in the 9th–11th centuries, cold anomalies in the 17th century, warm again in the 20th century) there is notable small-scale spatial variability among the individual proxies.

Temperatures from the 9th to 12th centuries are generally above the long-term mean, gradually cooling to below the mean in the 16th to 19th centuries and reaching a

CPD
7, 3349–3397, 2011

maximum cooling in the 17th century. The 20th century warming raised the centennial mean back to a level comparable to that of the 9th to 11th centuries. The resulting maps (Fig. 3) reveal remarkable large-scale spatial coherency of warm and cold conditions over the NH land areas for the past twelve centuries. The dominance of warm anomalies during the MWP and cold anomalies during the LIA is substantiated by results from the sign test (Fig. B1) that shows where and when there is significant agreement between the sign, positive or negative, of the proxies within their search radius (for more details see Appendix B).

The tests of robustness (see the accompanying supplement to this article) clearly reveal that when the spatial coverage decreases as proxies are excluded, the remaining spatial patterns of warm and cold anomalies are not substantially different from when all proxies are used. For example, the requirement that the proxies used must have data up to 1995 reduces the number of usable proxies to 34 yet, for the limited areas still covered, the overall patterns remain the same (compare Fig. 3 with Fig. S12 in the Supplement). Together the various experiments indicate that the observed large-scale spatial patterns of reconstructed normalized temperature anomalies, as seen in Fig. 3, are a robust feature of NH temperature variability over the last twelve centuries. Such an approach to assessing robustness is only possible with a large number of proxy records. Additionally, averaged time-series of centennial anomalies for subsets of proxies grouped by type, continent, latitude and seasonality of signal (Fig. 4) reveal essentially the same overall temporal trend with the exception of those proxy groups that have insufficient 20th century data (mainly pollen and sea sediment records).

Computing the rate of change within the last twelve centuries produces eleven maps of centennial first differences (Fig. 5). These maps show that the greatest rate of change over a widespread area was largest between the 19th and 20th centuries where strong warming is observed over nearly all areas with sufficient data. Comparable rates of warming between consecutive centuries are only seen for limited regions such as over Greenland from the 9th to the 10th century. The second largest geographical extensive warming between consecutive centuries occurs from the 17th to the

CPD
7, 3349–3397, 2011

18th centuries when almost all of North America, and much of the eastern half of Asia, warmed. A cooling trend is seen for most regions between the 10th and 13th centuries. The most widespread cooling between two consecutive centuries is from the 16th to the 17th.

4 Discussion

The density of proxies is comparatively high over Europe, Greenland, China and parts of North America, implying that the observed patterns over those regions are the most robust. The coverage is sparse over interior Asia and non-existent in North Africa and the Middle East. Consequently, these areas are either poorly replicated or left blank on the maps which is unfortunate as these are regions important to understanding teleconnection patterns in the climate system (e.g. El Niño/La Niña-Southern Oscillation and drought over southwestern North America, North Atlantic Oscillation and drought over China) (Graham et al., 2011; Lee and Zhang, 2011). More temperature proxies are thus needed, particularly in the interior of Asia, the Middle East, and northern Africa to firmly assess past climate variability. It is also essential to reconstruct climate patterns in the Southern Hemisphere (SH) and over the oceans in order to better understand the dynamics of internal variability and external forcings on global climate. This is presently difficult to achieve due to the scarcity of marine and SH proxy data.

Our reconstructed spatial anomalies cannot directly be compared with the calibrated climate field reconstruction by Mann et al. (2009) but we observe that our reconstructed patterns are not in disagreement. It is worth noting that our anomaly differences in the 9th to 11th centuries looks very similar to the MWP-LIA difference in Mann et al. (2009) where the influence of their 1961–1990 baseline period is removed (Fig. 6).

Analyses of instrumental data (Brohan et al., 2006) shows that the last decade of the 20th century was much warmer than the 20th century mean nearly everywhere over NH land areas with sufficient data (Fig. C1). Moreover, the first decade of the 21st century was even warmer in most locations thus providing evidence that the

CPD
7, 3349–3397, 2011

long-term, large-scale, NH warming that began in the 17th century and accelerated in the 20th century has continued unabated (see Appendix C for more details).

The warming from the 17th to the 20th century did not occur uniformly or simultaneously over all NH land regions (Figs. 3 and 5). Almost all of North America, western Europe and much of central and eastern Asia warmed from the 17th to the 18th century but not Greenland, Eastern Europe and northwestern Asia. Notable cooling occurred from the 18th to 19th century in northern Europe and much of Asia except in the south to southwest. This cooling caused the 19th century to be the coldest over much of northwestern Eurasia. Only from the 19th to the 20th century is warming observed over nearly all areas. Notable changes between consecutive centuries are also observed before the 17th century but these are more characterized by variability within smaller regions and no clear large-scale spatial patterns emerge apart from the overall long-term cooling from the 10th to the 17th century.

5 Conclusions

A principal importance of this study is that it proves that the science of paleoclimatology, particularly the collection and interpretation of proxy records, is capable of producing a body of evidence that can reveal many details of climate variability over time and space. Our results show, in a comparative manner, the degree to which the various proxy types can be used to assess regional temperature variability on centennial timescales. We conclude that during the 9th to 11th centuries there was widespread NH warmth comparable in both geographic extent and level to that of the 20th century mean. Our study also reveals that the 17th century was dominated by widespread and coherently cold anomalies representing the culmination of the LIA. Understandably, the centennial resolution of this study precludes direct comparison of past warmth to that of the last few decades. However, our results show the rate of warming from the 19th to the 20th century is clearly the largest between any two consecutive centuries in the past 1200 years.

CPD
7, 3349–3397, 2011

It is clear that not all proxies from the same local need exhibit the same centennial signal to infer a robust, regional, climate pattern provided a sufficient number of proxies are available to compute a meaningful average. For the same reason it is also clear that the choice of proxies used does not significantly change the overall conclusions of this study. Even after removing a significant number of proxies within the various tests of robustness, the significant spatial patterns of warm and cold anomalies remain the same as when all 120 proxies are used. This implies that our results depicting the large-scale spatial-temporal patterns of warm and cold conditions, as revealed by using all available temperature sensitive proxy records, can be considered as a robust reconstruction of the thermal conditions over the Northern Hemisphere over the last 12 centuries.

Appendix A

Methods and materials

A1 Proxy data

The peer-reviewed literature was systematically searched for all reported temperature proxy records spanning at least the 11th to 19th centuries and considered by their authors to be primarily a quantitative measure of local and/or regional temperature variability. Only records with at least two observations per century were considered. The large majority of raw data were either obtained from public databases (e.g. http://www.ncdc.noaa.gov/paleo/ and http://www.pangaea.de/) or by direct request from their authors. Those data that could not be had in either of the aforementioned ways were obtained by digitizing the figures where the data were published. The longitude, latitude, proxy type, sample resolution, seasonality and original reference of all 120 proxy records used are given in Table A1. The location of all the different proxy records is given in Fig. 1.

CPD
7, 3349–3397, 2011

The proxy data are divided the data into eight different categories: (1) Documentary, (2) Ice-core, (3) Lake sediments, (4) Pollen, (5) Sea sediments, (6) Speleothems, (7) Tree-rings, and (8) Other. All types of information from historical records used to reconstruct past temperatures are included in the category Documentary. The category Ice-core only includes δ^{18}O ice-core records. In the category Lake sediments all archives from lakes and peat bogs, excluding any pollen records, are included. The Pollen category includes all pollen records regardless of whether the pollen is derived from lake sediments, peat layers, ice-cores, or sea sediments. Sea sediments include all sediment records that are stated to reflect sea surface temperature. The category Speleothems includes δ^{18}O records and annual layer thickness from speleothems. The category Tree-rings includes tree-ring width and maximum latewood density (MXD) chronologies but not stable isotope records. Those proxies that did not fit into one of the above seven data categories were placed in the category "Other". This data category includes fossil wood remains, indicating changes in tree-line elevation, δ^{13}C tree-ring records and a N_2 and Ar isotopic ice-core record.

For the purpose of simplification we have collated the proxy data into three categories of seasonal temperature response: annual, winter, and summer temperature. Documented spring and early autumn temperature proxies are considered summer season records. Proxies expressing a late autumn season signal are included in the winter category. Records reflecting only spring or autumn temperature were so few that it was deemed inadequate to create separate categories for them. If no information on a proxy record's seasonality was available we assumed the proxy to be an annual mean temperature record. We recognize that Greenland δ^{18}O ice-core records, though stated to be a measure of annual mean temperature and used as such in this experiment, may actually be dominated by a winter temperature signal (Vinther et al., 2010).

In those cases where there exist multiple versions of a proxy record from the same site (e.g. the Torneträsk tree-ring record) the latest published version has been used. Whenever possible, preference was given to the highest resolution record available. If

CPD
7, 3349–3397, 2011

a tree-ring record exists both as a chronology of tree-ring widths and MXD we used the MXD record since this measure has stronger correlations to temperature (Briffa et al., 2002) and is generally reported as an integration of the whole growing season, whereas tree-ring width records primarily reflect conditions in the warmest months of the growing season (Tuovinen et al., 2009).

A2 Centennial variability and normalization of proxy records

The proxies' observational sampling rates vary from annual to a minimum of two observations per century. Prior to fitting a 167-year interpolative cubic smoothing spline, a frequency response equivalent to that of a 100-year moving average, those proxies with other than annual resolution are converted to an annually resolved time-series using simple linear interpolation. Once annually resolved the spline is fit to the interpolated data and every 25th spline value from the year 850 AD to 1950 AD is retained. These 45 spline values become a new time-series representing the average centennial temperature variability as expressed by the proxy. The 45 spline values are further normalized by their mean and standard deviation over a base period defined as the 11th to the 19th centuries (i.e. the mean and standard deviation for the 33 spline values at the time points 1050 AD, 1075 AD, ..., 1850 AD). Twelve of the 45 centennial anomalies, those at the time points 850 AD, 950 AD, ..., 1950 AD, representing the 9th to 20th centuries, are the centennial anomalies presented in the many maps throughout this experiment. Two examples that illustrate the pre-processing procedure are given in Figs. S1 and S2 in the Supplement.

A3 Correlation decay length of centennial temperature variability and anisotropic search radii

In order to find an appropriate search distance for the spatial averaging, the sign test and producing maps of gridded anomalies we need to consider the correlation decay structure of centennial temperatures and the spatial density of the available proxy data

CPD
7, 3349–3397, 2011

set. The correlation of temperature variability at different locations on the earth's surface typically decreases with increasing distance between locations. This correlation decay may be expressed as a negative exponential equation of the form

$$r = e^{-x/x_0}. \quad \text{(A1)}$$

Here, r is the correlation between temperature variations at distinct locations, x is the distance between the locations, and x_0 is the characteristic correlation decay length (CDL). The rate at which the correlation decay takes place is dependent on the time scale of the variations; the correlation decays slower for longer than for shorter timescales. The CDL also varies geographically and between seasons (Jones et al., 1997).

For the current study it is useful to have some knowledge about the CDL of centennial temperature variability because this helps determine the size of geographic regions/areas within which climate can be assumed to behave similarly. If the proxies within a CDL-defined region contain a meaningful temperature signal one would expect, when it was anomalously cold (or warm), the majority of within-area proxies will respond similarly. Therefore, the mean temperature anomaly, calculated from all proxies within the CDL-region, should be a fair estimate of central tendency for that region.

The CDL-region should be small enough to ensure that the real centennial temperature (within-area) variability is preserved and large enough to capture a sufficiently large number of proxies for calculating meaningful areal averages. However, the regions should not be so large that spatial details of temperature variability across the hemisphere cannot be distinguished. Hence, the determination of the size of the region must be based on a judgment that takes into account both the spatial distribution and density of the available proxies and some knowledge about the correlation decay structure for centennial temperature variations.

Unfortunately the CDL for centennial mean temperatures is not well known, as it cannot be estimated directly from the comparatively short instrumental record. Hence, climate model simulations are needed to help obtain some estimates. Jones et al. (1997)

CPD
7, 3349–3397, 2011

studied global patterns of the CDL from both an instrumental observational data set and in three climate model simulations at inter-annual and decadal time-scales. They also analyzed the CDL on centennial time-scales from one model simulation. Their study reveals that the CDL for internal variability, seen in control simulations, is typically shorter than that seen for externally forced simulations and shorter than in the instrumental observations – which must be assumed to contain a certain amount of externally forced variability. Different climate models provide different CDL values. Hence it is not possible to uniquely determine the structure of CDL for centennial temperature variations directly. However, Table 1 in Jones et al. (1997) suggests that the global mean value of CDL for unforced decadal variability, based on the two models that apparently produced the most realistic results, is on the order of ∼2000 km for annual mean temperatures and ∼1500 km for summer temperatures (which is the season with the shortest CDL). Certainly, the global mean value of CDL for real centennial temperatures must be longer. Table 5 in Jones et al. (1997) suggests that it could be on the order of ∼75 % longer than that for decadal temperatures. The CDL, however, varies geographically and is typically longer at the equator than at the pole.

To determine the size of regions within which centennial temperature variability can be expected to be rather strongly, positively, correlated one should choose regions where the distance between the center and periphery, i.e. the search radius, is smaller than the CDL for centennial time-scales. Guided by the results in Jones et al. (1997) we conclude a flexible search radius of 2000 km at the equator, that is allowed to decrease linearly with latitude to 1000 km at the pole, is small enough to ensure that the mean centennial temperature variability at the search-center should be positively correlated with most locations within the search radius. Such an anisotropic search function can be expressed mathematically as:

$$R = \text{lat} \times \left(\frac{r_{\text{min}} - r_{\text{max}}}{90} \right) + r_{\text{max}}. \quad \text{(A2)}$$

Here, R is the radius of a circle centred on any proxy or latitude lat. in the NH, r_{min} is the radius of a circle centred on the North Pole, and r_{max} is the radius of a circle

CPD
7, 3349–3397, 2011

centred on the equator (Fig. A3). Such circles, with $r_{min} = 1000$ and $r_{max} = 2000$, are wide enough to capture a reasonably large number of proxies and small enough to ensure that large-scale spatial patterns in temperature variability can be distinguished and are thus used in our sign tests, spatial averaging and producing maps of gridded values as described below. (Note that if Eq. A2 is used in the Southern Hemisphere, the latitude must be given with its absolute (positive) value).

The relative weight given to each proxy decreases from 1 at the grid node to $e^{-2} \approx 0.14$ at the search periphery (Fig. A4), following the Gaussian weight function:

$$\text{weight} = e^{-2x^2/R^2}. \quad \text{(A3)}$$

Here, weight is the weight given to a proxy value located at distance x from a grid or proxy node and R is the radius of the search circle defined by Eq. (A2). The Gaussian weight function is chosen because the Gaussian filter is frequently used as a low-pass filter for noise suppression both in time-series analysis and image processing (Wessel and Smith, 1998). In our notation, the quantity $R/2$ corresponds to what is usually referred to as the standard deviation or the scale. In our application the scale varies between 1000 km at the equator and 500 km at the pole. What is important is that the weights decay from large values at the grid node to small values at the search periphery. This is well achieved by Eq. (A3).

A4 Anisotropic spatial smoothing

The same search and weight functions are also used for calculating weighted means of neighbouring proxy anomalies where an anisotropic search is centred over the location of each proxy as opposed to the nodes of a Cartesian coordinate system. A weighted mean of centennial anomalies for a proxy location is performed if there are two or more neighbouring proxies (within the search distance) and all proxies, including the center proxy, possess a value for the century being considered. Thus the minimum number of proxies contributing to any weighted-mean centennial anomaly is three. Using these criteria the maximum number of proxies contributing to a single weighted-mean

CPD
7, 3349–3397, 2011

centennial anomaly, given the length and spatial distribution of the data used in this experiment, is twenty (Fig. A6).

A5 Anisotropic spatial gridding

The gridding of proxy data over a polar projection of the NH is done using a modification of the near-neighbour algorithm. We employ an anisotropic search radius (Eq. A2) to compute the values at each node of a $1^\circ \times 1^\circ$ grid covering the hemisphere. Figure A5 illustrates the procedure; all centennial proxy anomaly values within the search radius from each grid node contributes to a weighted mean assigned to the node's location if there are two or more node-local proxies. The weights used are defined by Eq. (A3).

Appendix B

The sign test – a simple robust anomaly test

Figure B1 presents results of sign tests (Arbuthnott, 1710) showing the degree of spatial agreement, for each of the 12 centuries considered, of the signs of the anomalies among neighbouring proxies within an anisotropic search radius that decreases from 2000 km at the equator to 1000 km at the pole. The null hypothesis is that all the local proxy anomalies located within a given search circle, centred over each proxy, are equally likely to be positive as negative. If this hypothesis is true, then a strong majority in either direction is unlikely. Hence when such a majority is observed we reject the null hypothesis and conclude that the observed agreement between the proxy anomalies indicates the presence of a signal in this direction.

Using the significance level 5 % and a normal approximation one finds that the number of agreeing anomalies needed is $n/2 + \sqrt{n}$, or to put it differently, the number of disagreeing anomalies can be at most $n/2 - \sqrt{n}$. One of the assumptions underlying the sign test is that the observations are independent, which is difficult to verify in the

CPD
7, 3349–3397, 2011

present situation. For this reason the sign test should be viewed as a simple robust method for deciding which anomalies show reasonable agreement with their neighbours (Table B1).

The regional sign tests strengthen the overall impressions from Fig. 3, the widespread agreement of positive anomalies in the 10th century and negative anomalies in the 17th century. However, in the 20th century there is notably less widespread agreement on the sign of anomalies. In particular, proxies from land areas in and surrounding the North Atlantic region and western Asia do not agree that the last century, as a whole, was warmer than the 11th–19th century average. This lack of agreement on the sign in the 20th century should not be interpreted as the proxy's inability to capture the thermal state of the climate in the last century. The lack of agreement on the sign in the 20th century should not be taken to mean that the proxies fail to capture the thermal state of the climate in the last century. Rather, it tells us that the proxy values are sufficiently close to the mean over the nine-century long baseline period for a substantial number of them to end up on either side of the baseline period mean. However, not all proxy records that are used for the 20th century analysis have data that completely cover the last 15 years (1985–1999 AD). This period is known to have been warmer than the mean of the last century (Fig. C1). If all the proxy records had data up to the end of the last century, more widespread agreement of positive anomalies would be expected.

Appendix C

Spatial patterns of decadal mean temperatures in gridded instrumental observations

To obtain a visual comparison between the spatio-temporal patterns of NH centennial temperatures seen in the proxy data for the last twelve centuries and the instrumentally observed NH temperatures we plot, in a similar manner as in Fig. 2, the decadal means

CPD
7, 3349–3397, 2011

of the 5° × 5° grid box temperatures from the HadCRUT3 data set (Brohan et al., 2006). Figure C1 shows, for each of the last twelve decades, the temperature anomalies (in °C) for each grid box expressed as deviations from the 1900–1999 mean. Grid boxes located over ocean areas are masked for the sake of comparison. The decadal deviation is calculated and plotted wherever a grid box has 80 % or more monthly data in the period 1900–1999 and 80 % or more monthly data in the decade in question.

A widespread NH warming since the late 19th century is clearly illustrated in the maps. The regions with sufficient data show that the 1890s to 1910s were colder than the 20th century mean and that the 1990s was the warmest decade in the last century. The first decade in the 21st century was more than 1 °C above the 20th century mean. At a few locations temperatures in the last decade were colder than the century mean. These are located in southern Greenland and North America. A well-documented early warm period is seen in the 1930s and 1940s, but the warmth in that period was not as geographically widespread as the post-1990 warmth. The last decade (2000–2009) was the warmest observed decade in the NH land areas and also the decade with the most widespread warmth.

Another obvious feature in Fig. C1 is that the spatial coherency of the instrumental decadal temperatures is clearly stronger than the proxy-based centennial temperature anomalies in Fig. 2. Because the spatial coherence is expected to increase with increasing time-scales this comparison reveals that the proxy series exhibit a substantial amount of noise which motivates the use of spatial averaging of proxy anomalies. In addition, the map in Fig. C1 shows us that the areas with poor coverage of instrumental temperature observations are often the same areas as those where proxy data are lacking. Consequently, even if new proxy series are retrieved from areas currently devoid of proxy information, it will still be difficult to calibrate them.

Supplementary material related to this article is available online at: http://www.clim-past-discuss.net/7/3349/2011/cpd-7-3349-2011-supplement.zip.

CPD
7, 3349–3397, 2011

Acknowledgements. We thank the Swedish Research Council (grants 70454201 and 90751501) and the European Union (FP6 grant 017008, "Millennium" project) for funding. Many thanks are due to Ed Cook for his discussion and comments. We are especially thankful to all those researchers who have provided us with un-archived proxy data and the many who have contributed their data to the World Data Center for Paleoclimatology and similar public data bases without which studies like this would not be possible.

References

Akima, H.: A new method of interpolation and smooth curve fitting based on local procedures, J. Assoc. Comput. Mach., 17, 589–602, 1970.

Andersson, C., Pausata, F. S. R., Jansen, E., Risebrobakken, B., and Telford, R. J.: Holocene trends in the foraminifer record from the Norwegian Sea and the North Atlantic Ocean, Clim. Past, 6, 179–193, doi:10.5194/cp-6-179-2010, 2010.

Arbuthnott, J.: An argument for Divine Providence, taken from the constant regularity observed in the births of both sexes, Philos. Trans., 27, 186–190, 1710.

Barron, J. A. and Bukry, D.: Solar forcing of Gulf of California climate during the past 2000 yr suggested by diatoms and silicoflagellates, Mar. Micropaleontol., 62, 115–139, 2007.

Bergthorsson, P.: An estimate of ice drift and temperature in 1000 years, Jökull, 19, 94, 1969.

Bernabo, J. C.: Quantitative estimates of temperature changes over the last 2700 years in Michigan based on pollen data, Quaternary Res., 15, 143–159, 1981.

Bird, B. W., Abbott, M. B., Finney, B. P., and Kutchko, B.: A 2000 year varve-based climate record from the central Brooks Range, Alaska, J. Paleolimnol., 41, 25–41, 2008.

Black, D. E., Abahazi, M. A., Thunell, R. C., Kaplan, A., Tappa, E. J., and Peterson, L. C.: An 8-century tropical Atlantic SST record from the Cariaco Basin: Baseline variability, twentieth-century warming, and Atlantic hurricane frequency, Paleoceanography, 22, PA4204, doi:10.1029/2007PA001427, 2007.

Bradley, R. S.: Paleoclimatology: Reconstructing climates of the Quaternary, Academic Press, San Diego, CA, 1999.

Bradley, R. S., Hughes, M. K., and Diaz, H. F.: Climate in medieval time, Science, 302, 404–405, 2003.

CPD

7, 3349–3397, 2011

Briffa, K. R.: Annual climate variability in the Holocene: interpreting the message of ancient trees, Quaternary Sci. Rev., 19, 87–105, 2000.
Briffa, K. R., Osborn, T. J., Schweingruber, F. H., Jones, P. D., Shiyatov, S. G., and Vaganov, E. A.: Tree-ring width and density data around the Northern Hemisphere: Part 1, local and regional climate signals, Holocene, 12, 737–757, 2002.
Briffa, K. R., Shishov, V. V., Melvin, T. M., Vaganov, E. A., Grudd, H., Hantemirov, R. M., Eronen, M., and Naurzbaev, M. M.: Trends in recent temperature and radial tree growth spanning 2000 years across northwest Eurasia, Philos. T. Roy. Soc. B, 363, 2271–2284, 2008.
Broecker, W. S.: Was the Medieval Warm Period global?, Science, 291, 1497–1499, 2001.
Brohan, P., Kennedy, J. J., Harris, I., Tett, S. F. B., and Jones, P. D.: Uncertainty estimates in regional and global observed temperature changes: a new data set from 1850, J. Geophys. Res., 111, D12106, doi:10.1029/2005jd006548, 2006.
Büntgen, U., Frank, D. C., Nievergelt, D., and Esper, J.: Summer temperature variations in the European Alps, A.D. 755–2004, J. Climate, 19, 5606–5623, 2006.
Büntgen, U., Tegel, W., Nicolussi, K., McCormick, M., Frank, D., Trouet, V., Kaplan, J. O., Herzig, F., Heussner, K.-U., and Wanner, H.: 2500 years of European climate variability and human susceptibility, Science, 331, 578–582, 2011.
Christiansen, B. and Ljungqvist, F. C.: Reconstruction of the extra-tropical NH mean temperature over the last millennium with a method that preserves low-frequency variability, J. Climate, accepted, 2011.
Clegg, B. F., Clarke, G. H., Chipman, M. L., Chou, M., Walker, I. R., Tinner, W., and Hu, F. S.: Six Millennia of Summer Temperature Variation Based on Midge Analysis of Lake Sediments from Alaska, Quaternary Sci. Rev., 29, 3308–3316, 2010.
Cook, T. L., Bradley, R. S., Stoner, J. S., and Francus, P.: Five thousand years of sediment transfer in a high arctic watershed recorded in annually laminated sediments from Lower Murray Lake, Ellesmere Island, Nunavut, Canada, J. Paleolimnol., 41, 77–94, 2009.
Corona, C., Edouard, J.-L., Guibal, F., Guiot, J., Bernard, S., Thomas, A., and Denelle, N.: Long-term summer (AD 751–2008) temperature fluctuation in the French Alps based on tree-ring data, Boreas, 40, 351–366, 2011.
Cronin, T. M., Dwyer, G. S., Kamiya, T., Schwede, S., and Willard, D. A.: Medieval Warm Period, Little Ice Age and 20th century temperature variability from Chesapeake Bay, Global Planet. Change, 36, 17–29, 2003.

CPD
7, 3349–3397, 2011

Crowley, T. J.: Causes of climate change over the past 1000 years, Science, 289, 270–277, 2000.
Crowley, T. J. and Lowery, T.: How Warm Was the Medieval Warm Period? A comment on "Man-made versus natural climate change", Ambio, 29, 51–54, 2000.
D'Andrea, W. J., Huang, Y., Fritz, S. C., and Anderson, N. J.: Abrupt Holocene climate change as an important factor for human migration in West Greenland, P. Natl Acad. Sci. USA, 108, 9765-9769, 2011.
D'Arrigo, R., Jacoby, G., Frank, D., Pederson, N., Cook, E., Buckley, B., Nachin, B., Mijiddorj, R., and Dugarjav, C.: 1738 years of Mongolian temperature variability inferred from a tree-ring width chronology of Siberian pine, Geophys. Res. Lett., 28, 543–546, 2001.
D'Arrigo, R., Wilson, R., and Jacoby, G.: On the long-term context for late twentieth century warming, J. Geophys. Res., 111, D03103, doi:10.1029/2005JD006352, 2006.
Diaz, H. F., Trigo, R., Hughes, M. K., Mann, M. E., Xoplaki, E., and Barriopedro, D: Spatial and temporal characteristics of climate in Medieval times revisited, B. Am. Meteorol. Soc., in press, 2011.
Divine, D., Isaksson, E., Martma, T., Meijer, H. A. J., Moore, J., Pohjola, V., van de Wal, R. S. W., and Godtliebsen, F.: Thousand years of winter surface air temperature variations in Svalbard and northern Norway reconstructed from ice core data, Polar Res., 30, 1–12, 2011.
Doose-Rolinski, H., Rogalla, U., Scheeder, G., Lücke, A., and von Rad, U.: High resolution temperature and evaporation changes during the late Holocene in the northeastern Arabian Sea, Paleoceanography, 16, 358–367, 2001.
Edwards, T. W. D., Birks, S. J., Luckman, B. H., and MacDonald, G. M.: Climatic and hydrologic variability during the past millennium in the eastern Rocky Mountains and northern Great Plains of western Canada, Quaternary Res., 70, 188–197, 2008.
Emeis, K. C. and Dawson, A. G.: Holocene palaeoclimatic records over Europe and the North Atlantic, Holocene, 13, 305–309, 2003.
Esper, J. and Frank, D. C.: IPCC on heterogeneous Medieval Warm Period, Climatic Change, 94, 267–273, 2009.
Esper, J., Cook, E. R., and Schweingruber, F. H.: Low-frequency signals in long tree-ring chronologies for reconstructing past temperature variability, Science, 295, 2250–2253, 2002.
Esper, J., Schweingruber, F. H., and Winiger, M.: 1300 years of climatic history for Western Central Asia inferred from tree-rings, Holocene, 12, 267–277, 2003.

CPD
7, 3349–3397, 2011

Filippi, M. L., Lambert, P., Hunziker, J., Kubler, B., and Bernasconi, S.: Climatic and anthropogenic influence on the stable isotope record from bulk carbonates and ostracodes in Lake Neuchatel, Switzerland, during the last two millennia, J. Paleolimnol., 21, 19–34, 1999.
Fisher, D. A., Koerner, R. M., Paterson, W. S. B., Dansgaard, W., Gundestrup, N., and Reeh, N.: Effect of wind scouring on climatic records from icecore oxygen isotope profiles, Nature, 301, 205–209, 1983.
Frisia, S., Borsato, A., Spötl, C., Villa, I. M., and Cucchi, F.: Climate variability in the SE Alps of Italy over the past 17 000 years reconstructed from a stalagmite record, Boreas, 34, 445–455, 2005.
Gajewski, K.: Late-Holocene climates of eastern North America estimated from pollen data, Quaternary Res., 29, 255–262, 1988.
Ge, Q., Zheng, J., Fang, X., Man, Z., Zhang, X., Zhang, P., and Wang, W.-C.: Winter half-year temperature reconstruction for the middle and lower reaches of the Yellow River and Yangtze River, China, during the past 2000 years, Holocene, 13, 933–940, 2003.
Geirsdóttir, A., Miller, G. H., Thordarson, T., and Ólafsdóttir, K. B.: A 2000 year record of climate variations reconstructed from Haukadalsvatn, West Iceland, J. Paleolimnol., 41, 95–115, 2009.
Goñi, M. A., Woodworth, M. P., Aceves, H. L., Thunell, R. C., Tappa, E., Black, D., Müller-Karger, F., Astor, Y., and Varela, R.: Generation, transport, and preservation of the alkenone-based $U_{37}K'$ sea surface temperature index in the water column and sediments of the Cariaco Basin (Venezuela), Global Biogeochem. Cy., 18, GB2001, doi:10.1029/2003GB002132, 2004.
Grootes, P. M. and Stuiver, M.: Oxygen 18/16 variability in Greenland snow and ice with 10^3 to 10^5-year time resolution, J. Geophys. Res., 102, 26455–26470, 1997.
Grove, J. M.: The Little Ice Age, 2nd Edn., Methuen, London, 1988.
Grudd, H.: Torneträsk tree-ring width and density AD 500–2004: a test of climatic sensitivity and a new 1500-year reconstruction of north Fennoscandian summers, Clim. Dynam., 31, 843–857, 2008.
Graumlich, L. J.: A 1000-yr record of temperature and precipitation in the Sierra Nevada, Quaternary Res., 39, 249–255, 1993.
Haltia-Hovi, E., Saarinen, T., and Kukkonen, M.: A 2000-year record of solar forcing on varved lake sediment in eastern Finland, Quaternary Sci. Rev., 26, 678, 2007.

CPD
7, 3349–3397, 2011

Hegerl, G., Crowley, T., Allen, M., Hyde, W., Pollack, H., Smerdon, J., and Zorita, E.: Detection of human influence on a new, validated, 1500 year temperature reconstruction, J. Climate, 20, 650–666, 2007.

Helama, S., Timonen, M., Holopainen, J., Ogurtsov, M. G., Mielikäinen, K., Eronen, M., Lindholm, M., and Meriläinen, J.: Summer temperature variations in Lapland during the Medieval Warm Period and the Little Ice Age relative to natural instability of thermohaline circulation on multi-decadal and multi-centennial scales, Quaternary Sci., 24, 450–456, 2009.

Hong, B., Liu, C.-Q., Lin, Q.-H., Yasuyuki, S., Leng, X.-T., Wang, Y., Zhu, Y.-X., and Hong, Y.-T.: Temperature evolution from the δ^{18}O record of Hani peat, Northeast China, in the last 14 000 years, Sci. China Ser. D, 52, 952–964, 2009.

Hong, Y. T., Jiang, H. B., Liu, T. S., Zhou, L. P., Beer, J., Li, H. E., Leng, X. T., Hong, B., and Qin, X. G.: Response of climate to solar forcing recorded in a 6000-year δ^{18}O time-series of Chinese peat cellulose, Holocene, 10, 1–7, 2000.

Hu, F. S., Ito, E., Brown, T. A., Curry, B. B., and Engstrom, D. R.: Pronounced climatic variations in Alaska during the last two millennia, P. Natl. Acad. Sci. USA, 98, 10552–10556, 2001.

Hughes, M. K. and Diaz, H. F.: Was there a "medieval warm period", and if so, where and when?, Climatic Change, 26, 109–142, 1994.

Jansen, E., Overpeck, J., Briffa, K., Duplessy, J.-C., Joos, F., Masson-Delmotte, V., Olago, D., Otto-Bliesner, B., Peltier, W., Rahmstorf, S., Ramesh, R., Raynaud, D., Rind, D., Solomina, O., Villalba, R., and Zhang, D.: Palaeoclimate, in: Climate Change 2007: The Physical Science Basis. Contribution of Working Group I to the Fourth Assessment Report of the Intergovernmental Panel on Climate Change, edited by: Solomon, S., Qin, D., Manning, M., Chen, Z., Marquis, M., Averyt, K., Tignor, M., and Miller, H., chap. 6, Cambridge University Press, Cambridge, UK and New York, NY, USA, 2007.

Jennings, A. E. and Weiner, N. J.: Environmental change in eastern Greenland during the last 1300 years: evidence from foraminifera and lithofacies in Nansen Fjord, 68° N, Holocene, 6, 179–191, 1996.

Jensen, K. G., Kuijpers, A., Koç, N., and Heinemeier, J.: Diatom evidence of hydrografhic changes and ice conditions in Igaliku Fjord, South Greenland, during the past 1500 years, Holocene, 14, 152, 2004.

Jiang, J., Eiriksson, M., Schultz, K. L., Knudsen, K.-L., and Seidenkrantz, S.: Evidence for solar forcing of sea surface temperature on the North Icelandic Shelf during the late Holocene, Geology, 33, 73–76, 2005.

CPD
7, 3349–3397, 2011

Jones, P. D. and Mann, M. E.: Climate over past millennia, Rev. Geophys., 42, RG2002, doi:10.1029/2003RG000143, 2004.
Jones, P. D., Osborn, T. J., and Briffa, K. R.: Estimating sampling errors in large-scale temperature averages, J. Climate, 10, 2548–2568, 1997.
Jones, P. D., Briffa, K. R., Barnett, T. P., and Tett, S. F. B.: High-resolution paleoclimatic records for the last millennium: Interpretation, integration and comparison with general circulation model control-run temperatures, Holocene, 8, 455–471, 1998.
Juckes, M. N., Allen, M. R., Briffa, K. R., Esper, J., Hegerl, G. C., Moberg, A., Osborn, T. J., and Weber, S. L.: Millennial temperature reconstruction intercomparison and evaluation, Clim. Past, 3, 591–609, doi:10.5194/cp-3-591-2007, 2007.
Kalugin, I. A., Daryin, A. V., and Babich, V. V.: Reconstruction of annual air temperatures for three thousand years in Altai region by lithological and geochemical indicators in Teletskoe Lake sediments, Dokl. Earth Sci., 426, 681–684, 2009.
Keigwin, L. D.: The Little Ice Age and Medieval Warm Period in the Sargasso Sea, Science, 274, 1504–1508, 1996.
Keigwin, L. D., Sachs, J. P., and Rosenthal, Y.: A 1600-year History of the Labrador Current off Nova Scotia, Clim. Dynam., 21, 53–62, 2003.
Kitagawa, H. and Matsumoto, E.: Climatic implications of δ^{13}C variations in a Japanese cedar (*Cryptomeria japonica*) during the last two millennia, Geophys. Res. Lett., 22, 2155–2158, 1995.
Klimanov, V. A., Khotinsky, N. A., and Blagoveshenskaya, N. V.: Climate fluctuations during the historical times in the center of Russian Plain, Izvestiya of Russian Academy of Sciences, Geographical Series, 1, 89, 1995.
Klimenko, V. V. and Sleptsov, A. M.: Multi-proxy reconstruction of the climate of Eastern Europe during the last 2,000 years, Izvestiya of the Russian Geographical Society, 6, 45–54, 2003.
Klimenko, V. V., Klimanov, V. A., Sirin, A. A., and Sleptsov, A. M.: Climate Changes in Western European Russia in the Late Holocene, Dokl. Earth Sci., 377, 190–194, 2001.
Kobashi, T., Severinghaus, J. P., Barnola, J.-M., Kawamura, K., Carter, T., and Nakaegawa, T.: Persistent multi-decadal Greenland temperature fluctuation through the last millennium, Climatic Change, 100, 733–756, 2010.
Lamb, H. H.: The early medieval warm epoch and its sequel, Palaeogeogr. Palaeocl., 1, 13–37, 1965.

CPD
7, 3349–3397, 2011

Lamoureux, S. F. and Bradley, R. S.: A late Holocene varved sediment record of environmental change from northern Ellesmere Island, Canada, J. Paleolimnol., 16, 239–255, 1996.
Lauritzen, S.-E. and Lundberg, J.: Calibration of the speleothem delta function: an absolute temperature record for the Holocene in northern Norway, Holocene, 9, 659–669, 1999.
Lee, H. F. and Zhang, D. D.: Relationship between NAO and drought disasters in northwestern China in the last millennium, J. Arid Environ., 75, 1114–1120, 2011.
Linderholm, H. W. and Gunnarson, B. E.: Summer temperature variability in central Scandinavia during the last 3600 years, Geogr. Ann. A, 87, 231–241, 2005.
Linge, H., Lauritzen, S.-E., Lundberg, J., and Berstad, I. M.: Stable isotope stratigraphy of Holocene speleothems: examples from a cave system in Rana, northern Norway, Palaeogeogr. Palaeocl., 167, 209–224, 2001.
Linge, H., Lauritzen, S.-E., Andersson, C., Hansen, J. K., Skoglund, R. Ø., and Sundqvist, H. S.: Stable isotope records for the last 10 000 years from Okshola cave (Fauske, northern Norway) and regional comparisons, Clim. Past, 5, 667–682, doi:10.5194/cp-5-667-2009, 2009.
Liu, Y., An, Z., Linderholm, H. W., Chen, D., Song, H., Cai, Q., Sun, J., Li, Q., and Tian, H.: Annual temperatures during the last 2485 years in the Eastern Tibetan Plateau inferred from tree rings, Sci. China Ser. D, 52, 348–359, 2009.
Liu, Z., Henderson, A. C. G., and Huang, Y.: Alkenone-based reconstruction of late-Holocene surface temperature and salinity changes in Lake Qinghai, China, Geophys. Res. Lett., 33, L09707, doi:10.1029/2006GL026151, 2006.
Ljungqvist, F. C.: A new reconstruction of temperature variability in the extra-tropical Northern Hemisphere during the last two millennia, Geogr. Ann. A, 92, 339–351, 2010.
Lloyd, A. H. and Graumlich, L. J.: Holocene dynamics of treeline forests in the Sierra Nevada, Ecology, 78, 1199–1210, 1997.
Loso, M. G.: Summer temperatures during the Medieval Warm Period and Little Ice Age inferred from varved proglacial lake sediments in southern Alaska, J. Paleolimnol., 41, 117–128, 2009.
Lou, J. Y. and Chen, C. T. A.: Paleoclimatological and palaeoenvironmental records since 4000 BP in the sediments of alpine lakes in Taiwan, Sci. China Ser. D, 40, 424–462, 1997.
Luckman, B. H. and Wilson, R. J. S., Summer temperatures in the Canadian Rockies during the last millennium: a revised record, Clim. Dynam., 24, 131–144, 2005.

CPD
7, 3349–3397, 2011

Lund, D. C. and Curry, W.: Florida Current surface temperature and salinity variability during the last millennium, Paleoceanography, 21, PA2009, doi:10.1029/2005PA001218, 2006.
Mangini, A., Spötl, C., and Verdes, P.: Reconstruction of temperature in the Central Alps during the past 2000 yr from a δ^{18}O stalagmite record, Earth Planet. Sc. Lett., 235, 741–751, 2005.
Mann, M. E. and Jones, P. D.: Global surface temperatures over the past two millennia, Geophys. Res. Lett., 30, 1820, doi:10.1029/2003GL017814, 2003.
Mann, M. E., Bradley, R. S., and Hughes, M. K.: Global-scale temperature patterns and climate forcing over the past six centuries, Nature, 392, 779–787, 1998.
Mann, M. E., Bradley, R. S., and Hughes, M. K.: Northern Hemisphere temperatures during the past millennium: Inferences, uncertainties, and limitations, Geophys. Res. Lett., 26, 759–762, 1999.
Mann, M. E., Zhang, Z., Hughes, M. K., Bradley, R. S., Miller, S. K., Rutherford, S., and Ni, F.: Proxy-based reconstructions of hemispheric and global surface temperature variations over the past two millennia, P. Natl. Acad. Sci. USA, 105, 13252–13257, 2008.
Mann, M. E., Zhang, Z., Rutherford, S., Bradley, R. S., Hughes, M. K., Shindell, D., Ammann, C., Faluvegi, G., and Ni, F.: Global signatures and dynamical origins of the Little Ice Age and Medieval Climate Anomaly, Science, 326, 1256–1260, 2009.
Martínez-Cortizas, A., Pontevedra-Pombal, X., Garcia-Rodeja, E., Novoa-Muñoz, J. C., and Shotyk, W.: Mercury in a Spanish peat bog: Archive of climate change and atmospheric metal deposition, Science, 284, 939–942, 1999.
Martín-Chivelet, J., Muñoz-García, M. B., Edwards, R. L., Turrero, M. J., and Ortega, A. I.: Land surface temperature changes in Northern Iberia since 4000 yr BP, based on δ^{13}C of speleothems, Global Planet. Change, 77, 1–12, 2011.
Matthews, J. A. and Briffa, K. R.: The Little Ice Age: Re-evaluation of an evolving concept, Geogr. Ann. A, 87, 17–36, 2005.
McKay, N. P., Kaufman, D. S., and Michelutti, N.: Biogenic silica concentration as a high-resolution, quantitative temperature proxy at Hallet Lake, south-central Alaska, Geophys. Res. Lett., 35, L05709, doi:10.1029/2007GL032876, 2008.
Millet, L., Arnaud, F., Heiri, O., Magny, M., Verneaux, V., and Desmet, M.: Late-Holocene summer temperature reconstruction from chironomid assemblages of Lake Anterne, northern French Alps, Holocene, 19, 317–328, 2009.

CPD
7, 3349–3397, 2011

Moberg, A., Sonechkin, D. M., Holmgren, K., Datsenko, N. M., and Karlén, W.: Highly variable Northern Hemisphere temperatures reconstructed from low- and high-resolution proxy data, Nature, 433, 613–617, 2005.
Moore, J. J., Hughen, K. A., Miller, G. H., and Overpeck, J. T.: Little Ice Age recorded in summer temperature reconstruction from varved sediments of Donard Lake, Baffin Island, Canada, J. Paleolimnol., 25, 503–517, 2001.
Naurzbaev, M. M., Vaganov, E. A., Sidorova, O. V., and Schweingruber, F. H.: Summer temperatures in eastern Taimyr inferred from a 2427-year late-Holocene tree-ring chronology and earlier floating series, Holocene, 12, 727–736, 2002.
NGRIP members: High-resolution record of Northern Hemisphere climate extending into the last interglacial period, Nature, 431, 147–151, 2004.
Nyberg, J., Malmgren, B. A., Kuijpers, A., and Winter, A.: A centennial-scale variability of tropical North Atlantic surface hydrography during the late Holocene, Palaeogeogr. Palaeocl., 183, 25–41, 2002.
Ojala, A. E. K. and Alenius, T.: 10,000 years of interannual sedimentation recorded in the Lake Nautajärvi (Finland) clastic-organic varves, Palaeogeogr. Palaeocl., 219, 285–302, 2005.
Oppo, D. W., Rosenthal, Y., and Linsley, B. K.: 2,000-year-long temperature and hydrology reconstructions from the Indo-Pacific warm pool, Nature, 460, 1113–1116, 2009.
Osborn, T. J. and Briffa, K. R.: The spatial extent of 20th-century warmth in the context of the past 1200 years, Science, 313, 841–844, 2006.
Park, J.: A modern pollen-temperature calibration data set from Korea and quantitative temperature reconstructions for the Holocene, Holocene, 21, 1125-1135, 2011.
Pla, S. and Catalan, J.: Chrysophyte cysts from lake sediments reveal the submillennial winter/spring climate variability in the northwestern Mediterranean region throughout the Holocene, Clim. Dynam., 24, 263–278, 2005.
Popa, I. and Kern, Z.: Long-term summer temperature reconstruction inferred from tree-ring records from the Eastern Carpathians, Clim. Dynam., 32, 1107–1117, 2009.
Qiang, M.-R., Chen, F.-H., Zhang, J.-W., Gao, S.-Y., and Zhou, A.-F.: Climatic changes documented by stable isotopes of sedimentary carbonate in Lake Sugan, northeastern Tibetan Plateau of China, since 2 ka BP, Chin. Sci. Bull., 50, 1930–1939, 2005.
Ran, L., Jiang, H., Knudsen, K. L. and Eiríksson, J.: Diatom-based reconstruction of palaeoceanographic changes on the North Icelandic shelf during the last millennium, Palaeogeogr. Palaeocl., 302, 109–119, 2011.

CPD
7, 3349–3397, 2011

Richey, J. N., Poore, R. Z., Flower, B. P., and Quinn, T. M.: 1400 yr multi-proxy record of climate variability from the northern Gulf of Mexico, Geology, 35, 423–426, 2007.
Salzer, M. W. and Kipfmueller, K. F.: Reconstructed temperature and precipitation on a millennial timescale from tree-rings in the Southern Colorado Plateau, U.S.A., Climatic Change, 70, 465–487, 2005.
Schmidt, R., Kamenik, C., and Roth, M.: Siliceous algae-based seasonal temperature inference and indicator pollen tracking ca. 4,000 years of climate/land use dependency in the southern Austrian Alps, J. Paleolimnol., 38, 541–554, 2007.
Sicre, M.-A., Hall, I. R., Mignot, J., Khodri, M., Ezat, U., Truong, M.-X., Eiríksson, J., and Knudsen, K.-L.: Sea surface temperature variability in the subpolar Atlantic over the last two millennia, Paleoceanography, accepted, 2011.
Solomina, O. and Alverson, K.: High latitude Eurasian paleoenvironments: introduction and synthesis, Palaeogeogr. Palaeocl., 209, 1–18, 2004.
Sümegi, P., Jakab, G., Majkut, P., Törőcsik, T., and Zatykó, C.: Middle Age palaeoecological and palaeoclimatological reconstruction in the Carpathian Sea, Időjárás, 113, 265, 2009.
Sundqvist, H. S., Holmgren, K., Moberg, A., Spötl, C., and Mangini, A.: Stable isotopes in a stalagmite from NW Sweden document environmental changes over the past 4000 years, Boreas, 39, 77–86, 2010.
Tan, M., Liu, T. S., Hou, J., Qin, X., Zhang, H., and Li, T.: Cyclic rapid warming on centennial-scale revealed by a 2650-year stalagmite record of warm season temperature, Geophys. Res. Lett., 30, 1617, doi:10.1029/2003GL017352, 2003.
Taricco, C., Ghil, M., Alessio, S., and Vivaldo, G.: Two millennia of climate variability in the Central Mediterranean, Clim. Past, 5, 171–181, doi:10.5194/cp-5-171-2009, 2009.
Thomas, E. K. and Briner, J. P.: Climate of the past millennium inferred from varved proglacial lake sediments on northeast Baffin Island, Arctic Canada, J. Paleolimnol., 41, 209–224, 2009.
Thompson, L. G., Mosley-Thompson, E., Brecher, H., Davis, M. E., Leon, B., Les, D., Mashiotta, T. A., Lin, P.-N. and Mountain, K.: Evidence of abrupt tropical climate change: past and present, P. Natl. Acad. Sci. USA, 103, 10536–10543, 2006.
Tiljander, M., Karhu, J. A., and Kauppila, T.: Holocene records of carbon and hydrogen isotope ratios of organic matter in annually laminated sediments of Lake Korttajärvi, central Finland, J. Paleolimnol., 36, 233–243, 2006.

CPD
7, 3349–3397, 2011

Treydte, K. S., Frank, D. C., Saurer, M., Helle, G., Schleser, G. H., and Esper, J.: Impact of climate and CO_2 on a millennium-long tree-ring carbon isotope record, Geochim. Cosmochim. Acta, 73, 4635–4647, 2009.

Tuovinen, M., McCarroll, D., Grudd, H., Jalkanen, R., and Los, S.: Spatial and temporal stability of the climatic signal in northern Fennoscandian pine tree ring width and maximum density, Boreas, 38, 1–12, 2009.

van Engelen, A. F. V., Buisman, J., and IJnsen, F.: A millennium of weather, winds and water in the Low Countrie, in: History and Climate: Memories of the Future?, edited by: Jones, P. D., Ogilvie, A. E. J., Davies, T. D., and Briffa, K. R., Kluwer Academic/Plenum Publishers, New York, Boston, Dordrecht, London, Moscow, 101–124, 2001.

Vinther, B. M., Clausen, H. B., Johnsen, S. J., Rasmussen, S. O., Andersen, K. K., Buchardt, S. L., Dahl-Jensen, D., Seierstad, I. K., Siggaard-Andersen, M.-L., Steffensen, J. P., Svensson, A. M., Olsen, J., and Heinemeier, J.: A synchronized dating of three Greenland ice cores throughout the Holocene, J. Geophys. Res., 111, D13102, doi:10.1029/2005JD006921, 2006.

Vinther, B. M., Clausen, H. B., Fisher, D. A., Koerner, R. M., Johnsen, S. J., Andersen, K. K., Dahl-Jensen, D., Rasmussen, S. O., Steffensen, J. P., and Svensson, A. M.: Synchronizing ice cores from the Renland and Agassiz ice caps to the Greenland Ice Core Chronology, J. Geophys. Res., 113, D08115, doi:10.1029/2007JD009143, 2008.

Vinther, B. M., Jones, P. D., Briffa, K. R., Clausen, H. B., Andersen, K. K., Dahl-Jensen, D., and Johnsen, S. J.: Climatic signals in multiple highly resolved stable isotope records from Greenland, Quaternary Sci. Rev., 29, 522–538, 2010.

Wanner, H., Beer, J., Bütikofer, J., Crowley, T., Cubasch, U., Flückiger, J., Goosse, H., Grosjean, M., Joos, F., Kaplan, J. O., Küttel, M., Müller, S., Pentice, C., Solomina, O., Stocker, T., Tarasov, P., Wagner, M., and Widmann, M.: Mid to late Holocene climate change – an overview, Quaternary Sci. Rev., 27, 1791–1828, 2008.

Wanner, H., Solomina, O., Grosjean, M., Ritz, S. P., and Jetel, M.: Structure and origin of Holocene cold events, Quaternary Sci. Rev., 30, 3109–3123, 2011.

Wessel, P. and Smith, W. H. F.: New, improved version of the Generic Mapping Tools Released, EOS Trans. AGU, 79, 579, 1998.

Wilks, D. S.: Resampling hypothesis tests for autocorrelated fields, J. Climate, 11, 65–82, 1997.

CPD
7, 3349–3397, 2011

Willemse, N. W. and Tornqvist, T. E.: Holocene century-scale temperature variability from West Greenland lake records, Geology, 27, 580–584, 1999.
Xu, Q. H., Xiao, J. L., Nakamura, T., Yang, X. L., Yang, Z. J., Liang, W. D., Inouchi, Y., and Yang, X. Y.: Quantitative reconstructed climatic changes of Daihai basin by pollen data, Mar. Geol. Quat. Geoi, 23, 99–108, 2003.
Yadav, R. R., Braeuning, A., and Singh, J.: Tree ring inferred summer temperature variations over the last millennium in western Himalaya, India, Clim. Dynam., 36, 1545–1554, 2011.
Zhang, Q., Gemmer, M., and Chen, J.: Climate changes and flood/drought risk in the Yangtze Delta, China, during the past millennium, Quaternary Int., 62, 176–177, 2008.
Zhang, Q.-B., Cheng, G., Yao, T., Kang, X., and Huang, J.: A 2,326-year tree-ring record of climate variability on the northeastern Qinghai-Tibetan Plateau, Geophys. Res. Lett., 30, 1739-1742, 2003.

CPD
7, 3349–3397, 2011

Table A1. All proxy records used in this study listed in geographical order from north to south.

Name	Longitude	Latitude	Type	Resolution	Season[a]	Reference
1. Lake C2	−77.54	82.47	Lake sediments	Annual	S	Lamoureux and Bradley (1996)
2. Lower Murray Lake	−69.32	81.21	Lake sediments	Annual	S	Cook et al. (2009)
3. Severnaja	106	81	Lake sediments	Multi-decadal	S	Solomina and Alverson (2004)[b]
4. Lomonosovfonna	17.42	78.85	Ice-cores	Sub-decadal	W	Divine et al. (2011)
5. Devon Island	−82.5	75.33	Ice-cores	Sub-decadal	A	Fisher et al. (1983)
6. NorthGRIP	−42.32	75.1	Ice-cores	Decadal	A	NGRIP members (2004)
7. GISP2	−38.5	72.6	Ice-cores	Annual	A	Grootes and Stuiver (1997)
8. GISP2	−38.5	72.6	Other	Annual	A	Kobashi et al. (2010)
9. GRIP	−37.38	72.35	Ice-cores	Annual	A	Vinther et al. (2010)
10. Crête	−37.32	71.12	Ice-cores	Annual	A	Vinther et al. (2010)
11. Renland	26.7	71.3	Ice-cores	Annual	A	Vinther et al. (2008)
12. Indigirka	148.15	70.53	Tree-rings	Annual	S	Solomina and Alverson (2004)[b]
13. Avam-Taimyr	93.00	70.00	Tree-rings	Annual	S	Briffa et al. (2008)
14. Big Round Lake	−68.50	69.83	Lake sediments	Annual	S	Thomas and Briner (2009)
15. Finnish Lapland	25.00	69.00	Tree-rings	Annual	S	Helama et al. (2010)
16. Laanila	27.30	68.50	Tree-rings	Annual	S	Lindholm et al. (2011)
17. Torneträsk	19.80	68.31	Tree-rings	Annual	S	Grudd (2008)
18. Nansen Fjord	−29.60	68.25	Sea sediments	Multi-decadal	S	Jennings and Weiner (1996)[b]
19. Blue Lake	−150.46	68.08	Lake sediments	Annual	S	Bird et al. (2009)
20. FM3	15.38	67.26	Speleothems	Multi-decadal	A	Linge et al. (2009)
21. Lake SFL4	−50.17	67.05	Lake sediments	Sub-decadal	S	Willemse and Tornqvist (1999)
22. Braya Sø	−50.42	67.00	Lake sediments	Multi-decadal	S	D'Andrea et al. (2011)
23. Yamal Penninsula	69.00	67.00	Other	Multi-decadal	S	Solomina and Alverson (2004)[b]
24. Core MD95-2011	7.64	66.97	Sea sediments	Multi-decadal	S	Andersson et al. (2010)
25. Yamal	69.17	66.92	Tree-rings	Annual	S	Briffa (2000)
26. Polar Urals	65.75	66.83	Tree-rings	Annual	S	Esper et al. (2002a)
27. Donard Lake	−61.35	66.66	Lake sediments	Annual	S	Moore et al. (2001)
28. North Iceland Shelf	−17.22	66.33	Sea sediments	Multi-decadal	W	Jiang et al. (2005)
29. North Iceland Shelf	−17.22	66.33	Sea sediments	Multi-decadal	S	Jiang et al. (2005)
30. Søylegrotta	13.55	66.33	Speleothems	Multi-decadal	A	Lauritzen and Lundberg (1999)
31. MD99-2275	−19.30	66.30	Sea sediments	Sub-decadal	S	Ran et al. (2011)
32. MD99-2275_45	−19.30	66.30	Sea sediments	Sub-decadal	S	Sicre et al. (2011)
33. SG95	13.55	66.33	Speleothems	Multi-decadal	A	Linge et al. (2009)
34. Dye-3	−43.49	65.11	Ice-core	Annual	A	Vinther et al. (2010)
35. Haukdalsvatn	−21.37	65.03	Lake sediments	Sub-decadal	S	Geirsdóttir et al. (2009)
36. Iceland	−18.00	65.00	Documentary	Multi-decadal	A	Bergthorsson (1969)[b]
37. Korallgrottan	14.16	64.89	Speleothems	Multi-decadal	A	Sundqvist et al. (2010)
38. Jämtland	13.30	63.10	Tree-rings	Annual	S	Linderholm and Gunnarson (2005)
39. Lake Lehmilampi	29	63	Lake sediments	Annual	A	Haltia-Hovi et al. (2007)
40. Farewell Lake	−153.63	62.55	Lake sediments	Multi-decadal	S	Hu et al. (2001)
41. Lake Korttajärvi	25.68	62.33	Lake sediments	Annual	A	Tiljander et al. (2006)
42. Hallet Lake	−146.20	61.50	Lake sediments	Sub-decadal	S	McKay et al. (2008)
43. Moose Lake	−143.61	61.37	Lake sediments	Multi-decadal	S	Clegg et al. (2010)
44. Lake Nautajärvi	24.68	61.80	Lake sediments	Annual	A	Ojala and Alenius (2005)
45. Iceberg Lake	−142.95	60.78	Lake sediments	Annual	S	Loso (2009)
46. Outer Igaliku Fjord	−46.00	60.40	Sea sediments	Multi-decadal	S	Jensen et al. (2004)[b]

CPD
7, 3349–3397, 2011

Table A1. Continued.

Name	Longitude	Latitude	Type	Resolution	Season[a]	Reference
47. Inner Igaliku Fjord	−46.00	60.40	Sea sediments	Multi-decadal	S	Jensen et al. (2004)[b]
48. Gulf of Alaska	−145	60	Tree-rings	Annual	S	D'Arrigo et al. (2006)
49. Polovetsko-Kupanskoye	38.7	56.94	Pollen	Multi-decadal	A	Klimanov et al. (1995)
50. Usvyatskii Mokh	32	56	Pollen	Multi-decadal	A	Klimenko et al. (2001)
51. Russian Plains	45.00	45.00	Other	Decadal	A	Klimenko and Sleptsov (2003)
52. Columbia Icefield	−117.15	52.15	Tree-rings	Annual	S	Luckman and Wilson (2005)
53. Columbia Icefield	−117.15	52.15	Other	Annual	W	Edwards et al. (2008)
54. DeBilt winter	5.18	52.1	Documentary	Multi-decadal	W	van Engelen et al. (2001)[b]
55. DeBilt winter	5.18	52.1	Documentary	Multi-decadal	S	van Engelen et al. (2001)[b]
56. Central England	1.00	52.00	Documentary	Multi-decadal	A	Lamb (1965)
57. Teletskoe Lake	87.61	51.76	Lake sediments	Annual	A	Kalugin et al. (2009)
58. Sol Dav	98.93	48.3	Tree-rings	Annual	S	D'Arrigo et al. (2001)
59. Nadas Lake	19.7	47.99	Pollen	Multi-decadal	A	Sümegi et al. (2009)[b]
60. Eastern Carpathians	25.10	47.20	Tree-rings	Annual	S	Popa and Kern (2009)
61. Oberer Landschitzsee	13.36	47.13	Lake sediments	Multi-decadal	S	Schmidt et al. (2007)
62. Spannagel Cave	11.4	47.05	Speleothems	Sub-decadal	A	Mangini et al. (2005)
63. Lake Neuchatel	6.7	46.8	Pollen	Multi-decadal	A	Filippi et al. (1999)[b]
64. The Alps	8.00	46.30	Tree-rings	Annual	S	Büntgen et al. (2006)
65. Conroy Lake	−67.88	46.28	Pollen	Multi-decadal	S	Gajewski (1988)
66. Marion Lake	−89.09	46.26	Pollen	Multi-decadal	S	Bernabo (1981)
67. Hells Kitchen Lake	−89.42	46.11	Pollen	Multi-decadal	S	Gajewski (1988)
68. Central Europe	8.00	46.00	Tree-rings	Annual	S	Büntgen et al. (2011)
69. French Alps	9.00	46.00	Tree-rings	Annual	S	Corona et al. (2011)
70. Grotta Savi	13.89	45.62	Speleothems	Decadal	A	Frisia et al. (2005)
71. Lake Anterne	6.47	45.59	Lake sediments	Multi-decadal	S	Millet et al. (2009)
72. Emerald Basin	−62.00	45.00	Sea sediments	Multi-decadal	A	Keigwin et al. (2003)
73. Basin Pond	−70.03	44.28	Pollen	Multi-decadal	S	Gajewski (1988)
74. Lake of the Clouds	−71.25	44.25	Pollen	Multi-decadal	S	Gajewski (1988)
75. Les Merveilles	7.45	44.03	Tree-rings	Annual	S	(ITRDB FRAN010)[c]
76. Idaho	−114.00	44.00	Tree-rings	Annual	S	(ITRDB ID009, ID010, and ID012)[c]
77. Clear Pond	−74.01	43.45	Pollen	Multi-decadal	S	Gajewski (1988)
78. Penido Vello	−7.34	43.32	Other	Multi-decadal	A	Martínez-Cortizas et al. (1999)
79. Northern Spain	−3.50	42.90	Speleothems	Multi-decadal	A	Martín-Chivelet et al. (2011)
80. Jones Lake	−84.56	42.77	Pollen	Multi-decadal	S	Bernabo(1981)[b]
81. Lake 27	−83.43	42.73	Pollen	Multi-decadal	S	Bernabo (1981)[b]
82. Lake Redon	0.77	42.64	Lake sediments	Multi-decadal	W	Pla and Catalan (2005)
83. Jinchuan	126.37	42.33	Lake sediments	Multi-decadal	A	Hong et al. (2000)
84. Hani	126.51	42.21	Lake sediments	Multi-decadal	A	Hong et al. (2009)[b]
85. Daihai Basin	112.68	40.57	Lake sediments	Multi-decadal	S	Xu et al. (2003)
86. Tien Shan	72.00	40.00	Tree-rings	Annual	S	Esper et al. (2003)[b]
87. Gulf of Taranto	17.88	39.75	Sea sediments	Multi-decadal	A	Taricco et al. (2009)
88. ShiHua Cave	115.56	39.47	Speleothems	Annual	S	Tan et al. (2003)
89. Chesapeake Bay	−76.40	39.00	Sea sediments	Multi-decadal	S	Cronin et al. (2003)
90. Hill 10842	−114.23	38.93	Tree-rings	Annual	S	(ITRDB NV516)[c]
91. Sugan Lake	93.9	38.85	Lake sediments	Multi-decadal	W	Qiang et al. (2005)

CPD
7, 3349–3397, 2011

Table A1. Continued.

Name	Longitude	Latitude	Type	Resolution	Season[a]	Reference
92. Dunde	96.40	38.10	Ice-cores	Decadal	A	Thompson et al. (2006)
93. Lucky Horseshoe	−118.33	37.87	Tree-rings	Annual	S	(ITRDB NV519)[c]
94. Glass Mountain	−118.68	37.75	Tree-rings	Annual	S	(ITRDB CA633)[c]
95. Sheep Mountain	−118.22	37.37	Tree-rings	Annual	S	(ITRDB CA534)[c]
96. M40-4-SL78	13.19	37.03	Sea sediments	Multi-decadal	A	Emeis and Dawson (2003)
97. Korea	128.00	37	Pollen	Multi-decadal	A	Park et al. (2011)[b]
98. Lake Qinghai	100	37	Lake sediments	Multi-decadal	A	Liu et al. (2006)
99. Southern Sierra Nevada	−118.90	36.90	Tree-rings	Annual	S	Graumlich (1993)
100. Tibet	98.5	36.5	Tree-rings	Annual	A	Liu et al. (2009)
101. Karakorum Mountains	74.99	36.37	Other	Annual	A	Treydte et al. (2009)
102. Upper Wright Lakes	−118.22	36.37	Tree-rings	Annual	S	Lloyd and Graumlich (1997)
103. Boreal Plateau	−118.33	36.27	Tree-rings	Annual	S	Lloyd and Graumlich (1997)
104. Dulan	98	36	Tree-rings	Annual	A	Zhang et al. (2003)
105. Guliya	81.48	35.28	Ice-cores	Decadal	A	Thompson et al. (2006)
106. Southern Colorado Plateau	−111.4	35.2	Tree-rings	Annual	S	Salzer and Kipfmueller (2005)
107. East China	114	35	Documentary	Multi-decadal	W	Ge et al. (2003)
108. Karakorum Mountains	76	35	Tree-rings	Annual	A	Esper et al. (2002b)
109. Bermuda	−57.63	33.72	Sea sediments	Multi-decadal	A	Keigwin (1996)
110. Western Himalaya	76.45	32.50	Tree-rings	Annual	S	Yadav et al. (2011)[b]
111. Yangtze Delta	121.0	32.0	Documentary	Decadal	A	Zhang et al. (2008)[b]
112. Yakushima Island	130.3	30.2	Other	Multi-decadal	A	Kitagawa and Matsumoto (1995)
113. Pigmy Basin	−91.42	27.2	Sea sediments	Multi-decadal	A	Richey et al. (2007)
114. Jiaming Lake	121.3	25.01	Lake sediments	Multi-decadal	A	Lou and Chen (1997)
115. SO90-39KG	65.92	24.83	Sea sediments	Multi-decadal	A	Doose-Rolinski et al. (2001)
116. Pescadero Basin	−108.2	24.27	Sea sediments	Multi-decadal	A	Barron and Bukry (2007)
117. Great Ghost Lake	120.51	22.52	Lake sediments	Multi-decadal	A	Lou and Chen (1997)
118. Caribbean Sea	−66.6	17.88	Sea sediments	Multi-decadal	A	Nyberg, et al. (2002)
119. Cariaco Basin	−64.56	10.42	Sea sediments	Multi-decadal	A	Goñi et al. (2004); Black et al. (2007)
120. Indo-Pacific Warm Pool	119.27	−3.53	Sea sediments	Sub-decadal	A	Oppo et al. (2009)

[a] A = Annual, S = Summer, W = Winter

Proxy records marked with [b] were digitized from publish figures.

[c] ITRDB = The International Tree-Ring Data Bank at the NOAA Paleoclimatology Program and World Data Center for Paleoclimatology (http://www.ncdc.noaa.gov/paleo/treering.html).

CPD
7, 3349–3397, 2011

Table B1. The maximum number of permissible disagreeing proxies (d) for a given number of total proxies (n) found within a search radius to pass the sign test.

n	3	4	5	6	7	8	9	10	11	12	13	14	15	16	17	18	19	20
d	0	0	0	1	1	1	2	2	2	3	3	3	4	4	4	5	5	6

CPD
7, 3349–3397, 2011

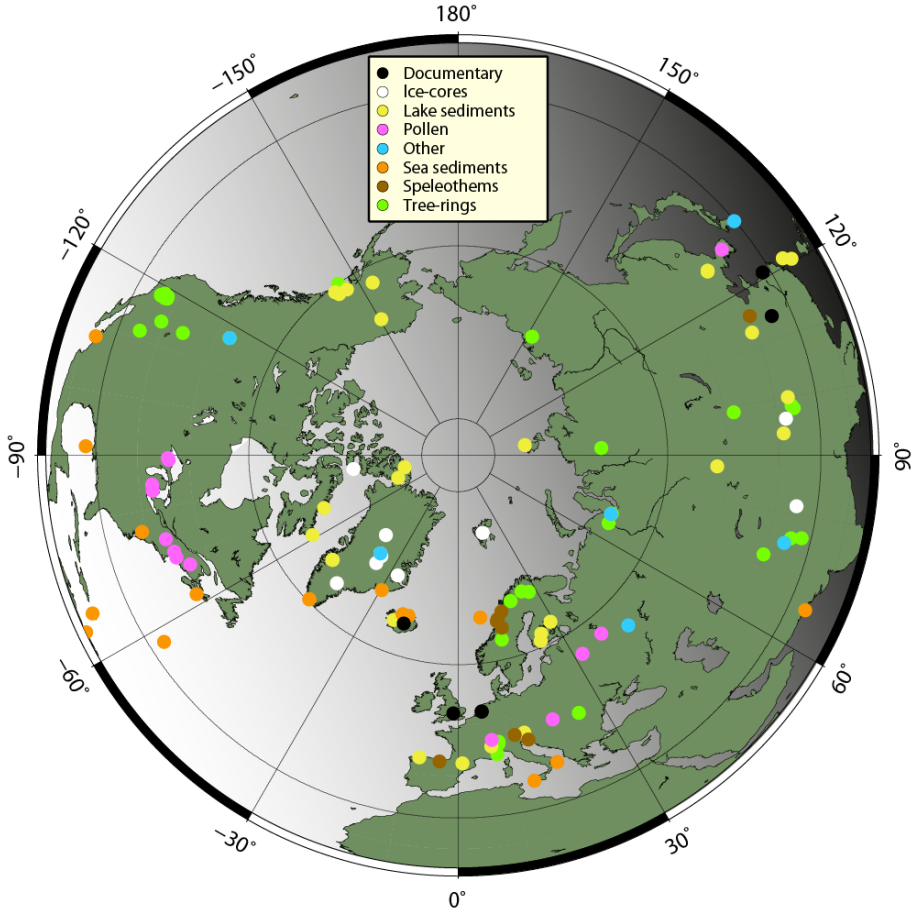

Fig. 1. Type and location of all 120 proxy records used in this study (see Table 1).

CPD
7, 3349–3397, 2011

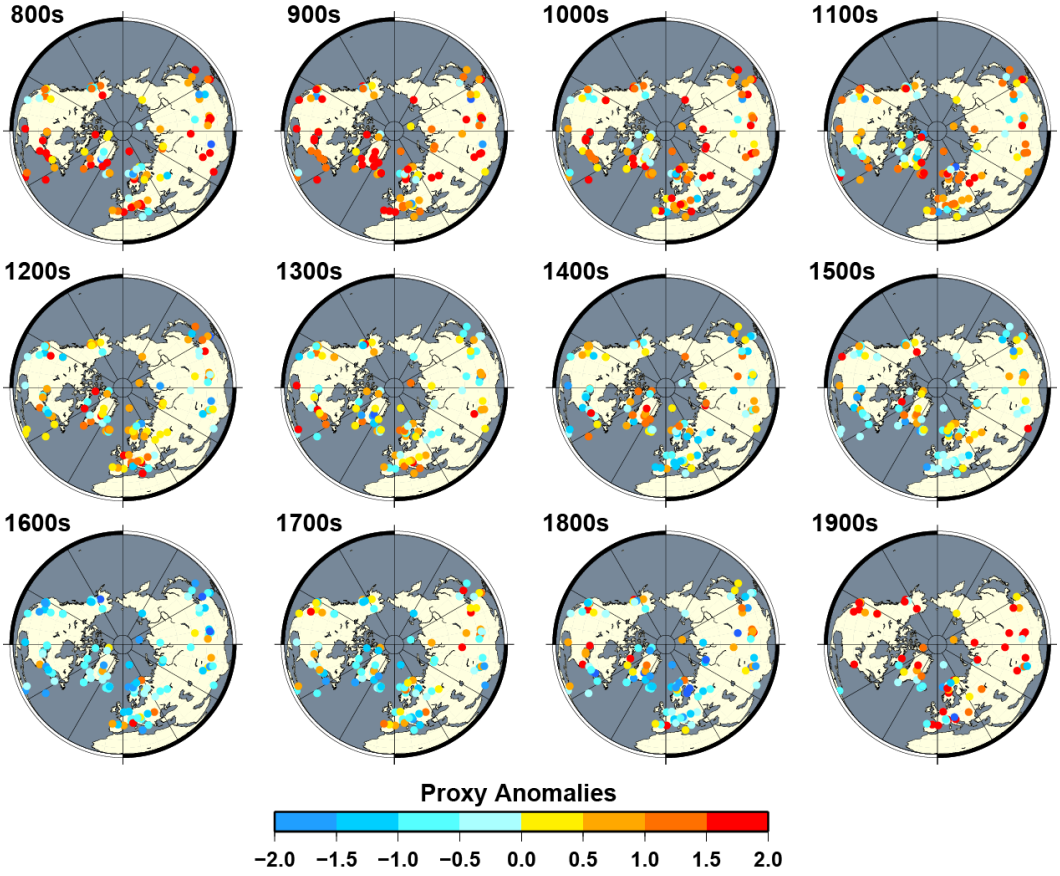

Fig. 2. Raw, centennial, proxy anomaly values. Anomalies are shown relative to the centennial mean and standard deviation over the 11th–19th centuries. The colour scale is truncated at −2 and 2.

CPD
7, 3349–3397, 2011

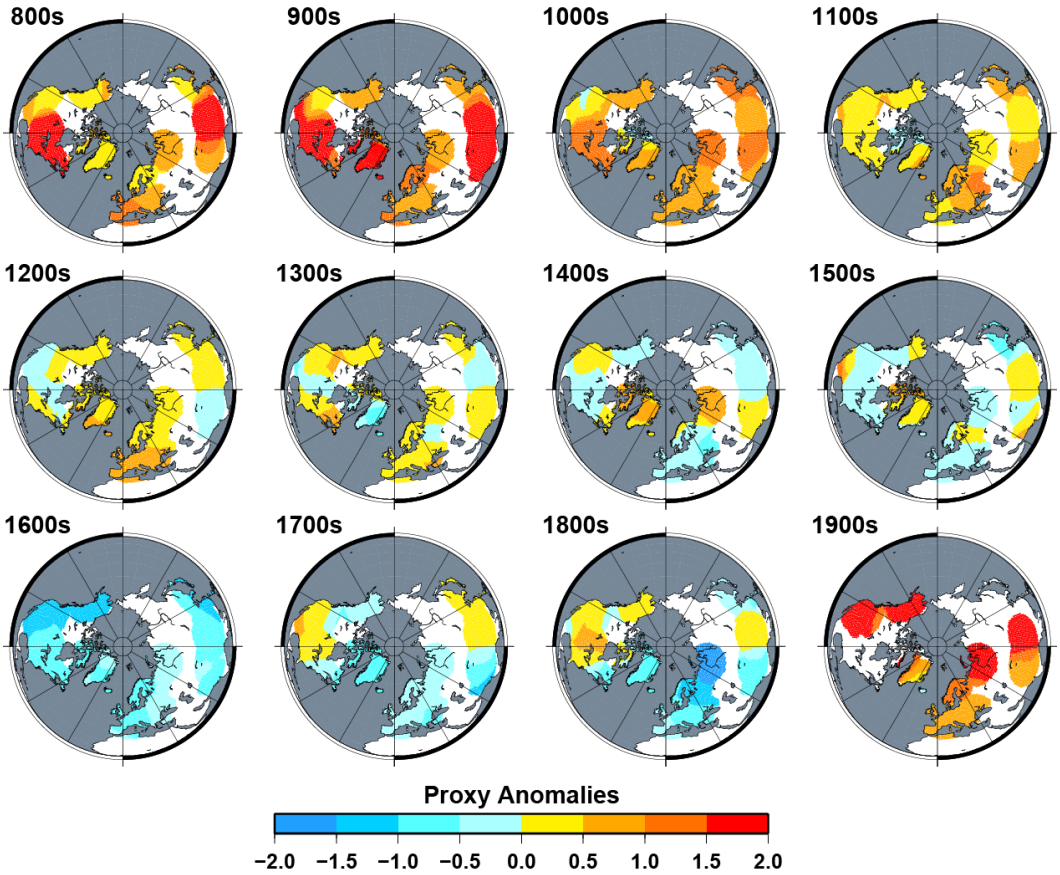

Fig. 3. Gridded, weighted, centennial proxy anomalies derived from the data shown in Fig. 1. Anomalies are shown relative to the 11th–19th century reference period. The colour scale is truncated at −2 and 2.

CPD
7, 3349–3397, 2011

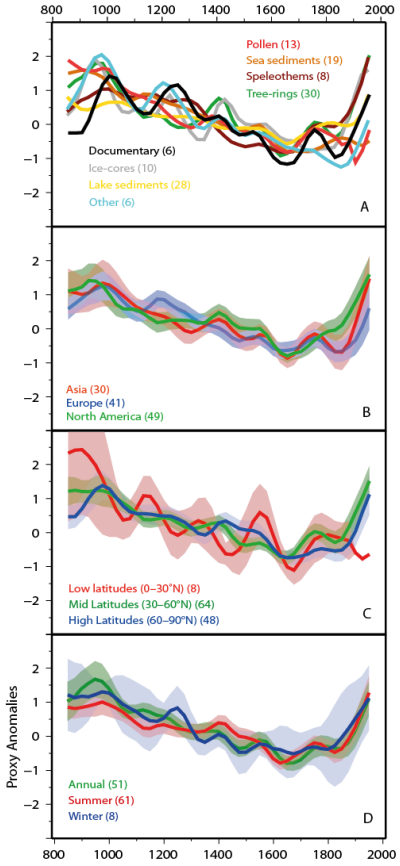

Fig. 4. Mean time-series of centennial proxy anomalies separated by: **(A)** data type, **(B)** continents, **(C)** latitude, **(D)** seasonality of signal. The curves in **(B)**–**(D)** show the mean and moving block bootstrap confidence intervals (±2 standard error) (Wilks, 1997). The numbers in parentheses indicates the number of proxies in each category.

CPD
7, 3349–3397, 2011

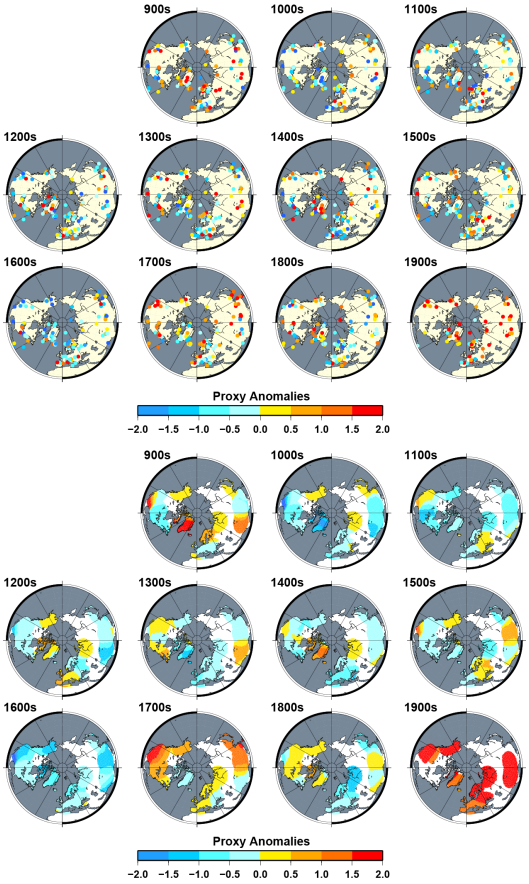

Fig. 5. Centennial first-differences between each century and the previous. Upper panel: Differences for raw centennial proxy anomaly values as shown in Fig. 2. Lower panel: gridded, weighted, centennial anomaly values for the same data. The colour scale in both panels is truncated at −2 and 2.

CPD
7, 3349–3397, 2011

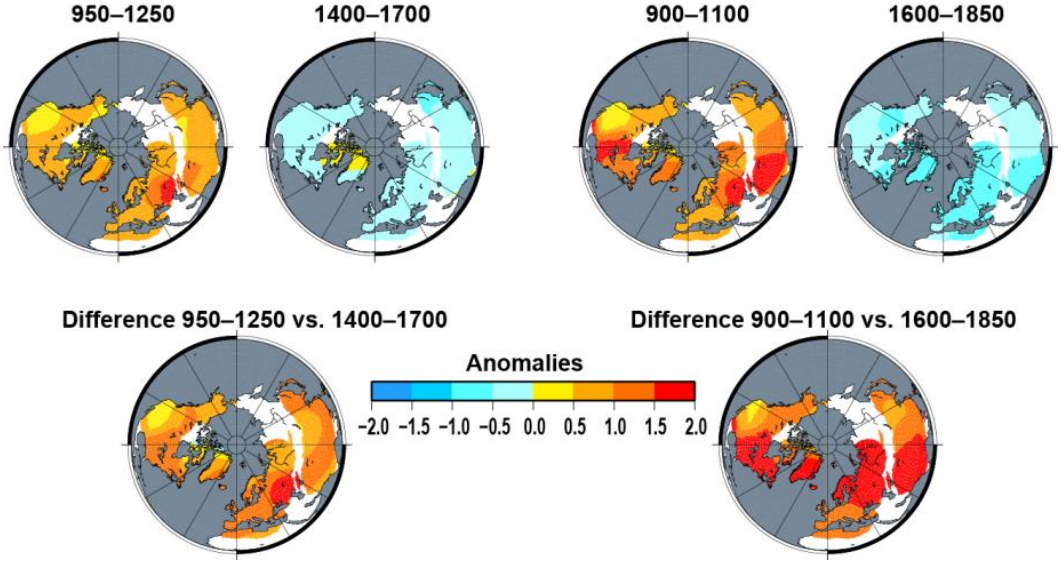

Fig. 6. The mean and differences in anomaly values from our spatial reconstruction using the same two MWP and LIA periods defined in Mann et al. (2009).

CPD
7, 3349–3397, 2011

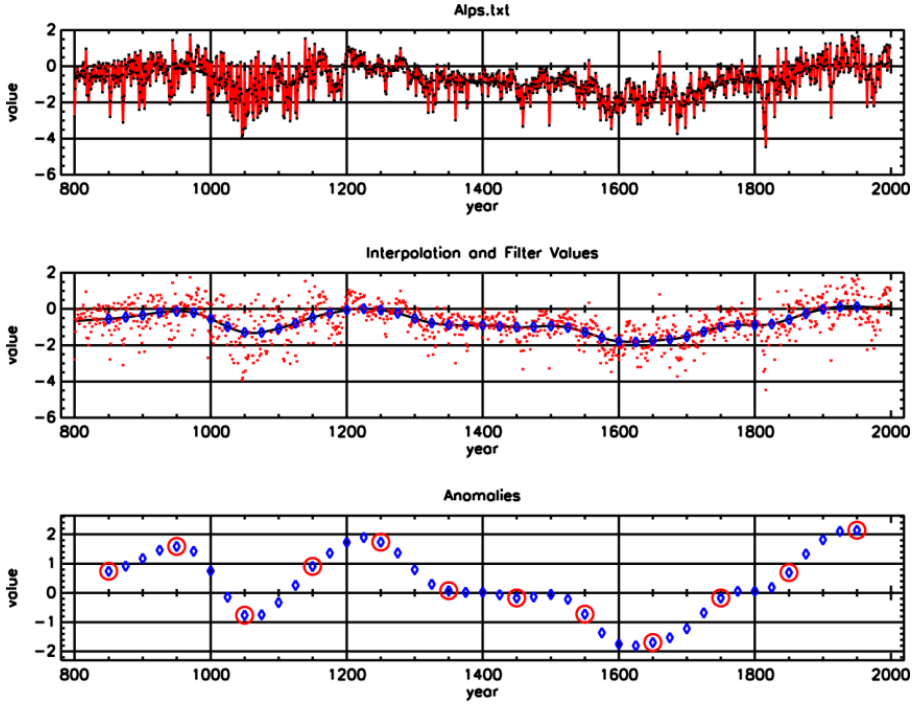

Fig. A1. Example illustrating the transformation of an annually resolved proxy record to a centennially resolved anomaly time series. The top panel shows the raw data, in original units, with its spline fit. The middle panel shows the raw data (red dots) and the 45, 100 year, moving averages (overlap = 25 year) between 850 AD and 1950 AD (blue diamonds). The bottom panel shows the 45, normalized (base period: 11th–19th centuries) centennial filter values (blue diamonds) and the values of the 12 common centuries (red circles).

CPD
7, 3349–3397, 2011

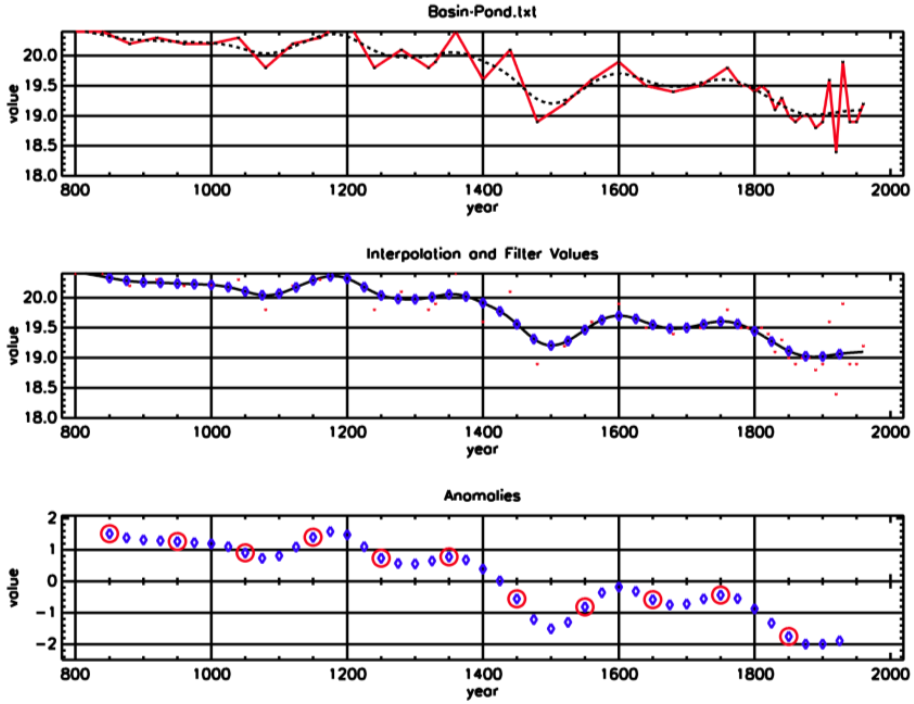

Fig. A2. An example illustrating the transformation of a non-annually resolved proxy record to a centennially resolved anomaly series. The top panel shows the raw data, in original units, with its spline fit. The middle panel shows the raw data (red dots) and the 45, 100 year, moving averages (overlap = 25 year) between 850 AD and 1850 AD (blue diamonds). The bottom panel shows the 45, normalized (base period: 11th–19th centuries) centennial filter values (blue diamonds) and the values of the 12 common centuries (red circles).

CPD
7, 3349–3397, 2011

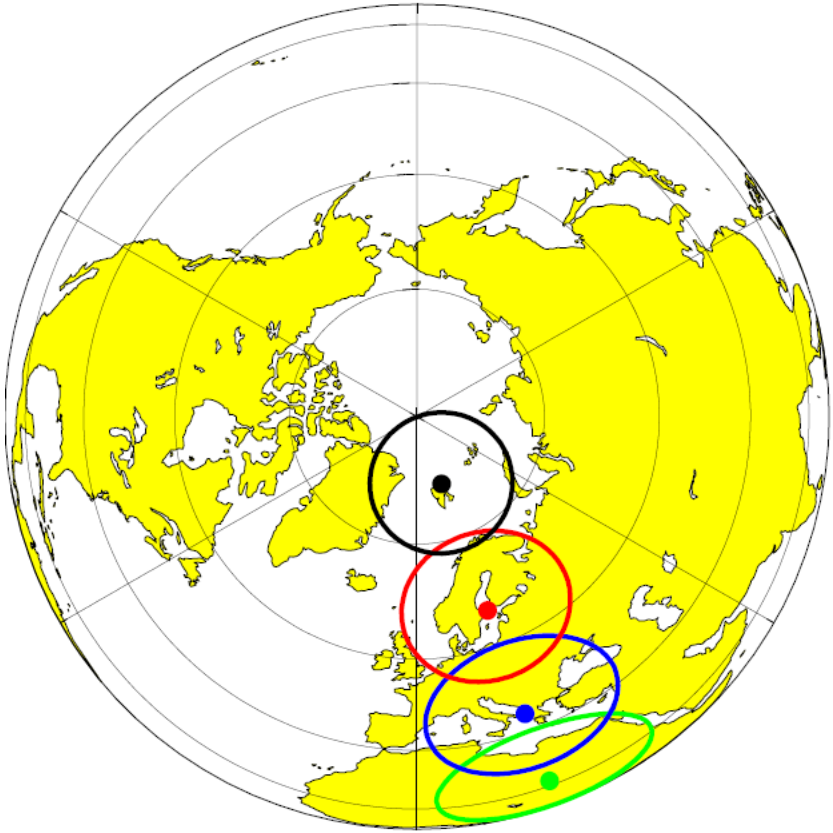

Fig. A3. Example of search circles used for sign tests, spatial averaging and gridding placed along 20° E. Their radii decrease linearly with latitude from 2000 km at the equator to 1000 km at the pole. The four circles illustrated are placed at 20°, 40°, 60° and 80° N and have radial distances of 1778 km, 1556 km, 1333 km and 1111 km, respectively. The apparently elliptic shape of the circles is a consequence of the map projection.

CPD
7, 3349–3397, 2011

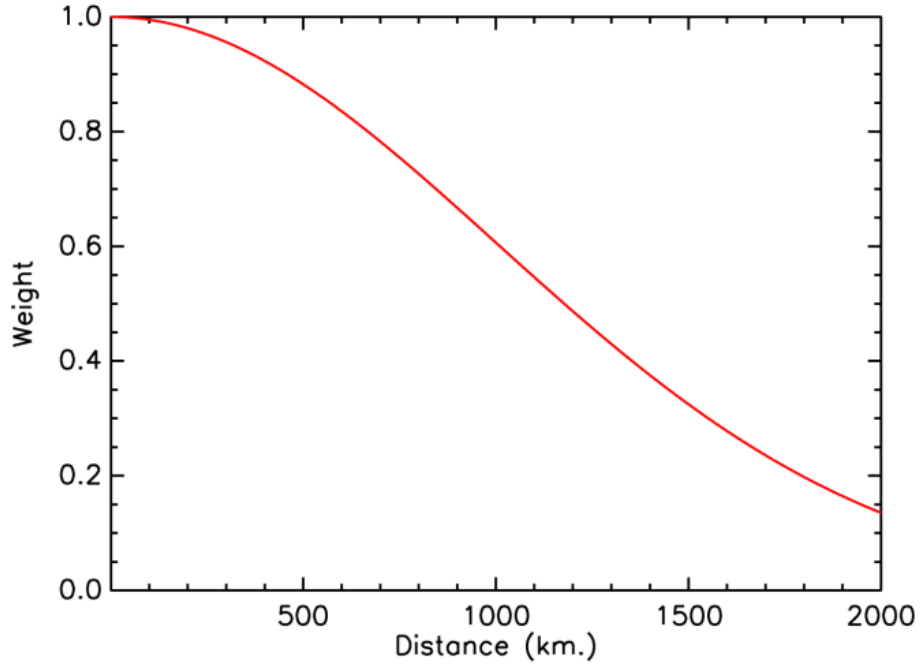

Fig. A4. The Gaussian weight function for proxies located at a distance of x km from a grid node, as derived from Eq. (A3), for an example search radius (R) of 2000 km.

CPD
7, 3349–3397, 2011

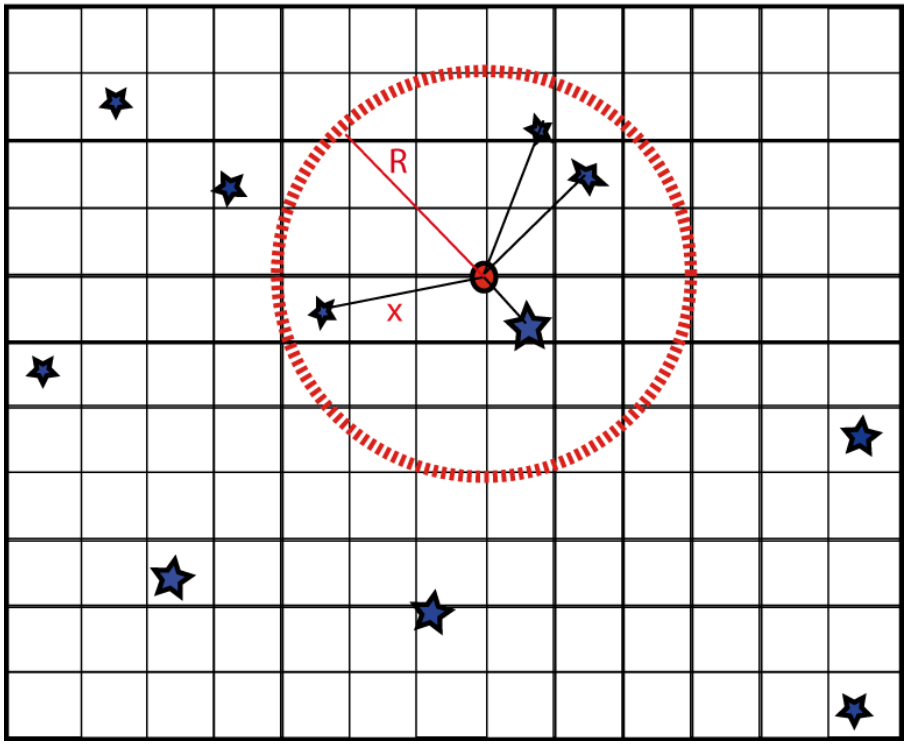

Fig. A5. Spatial gridding of centennial proxy anomalies on a 1° × 1° grid using a modified near-neighbour gridding algorithm. Capital *R* is the search radius from each grid node as computed by Eq. (A2) where lat is the latitude of the grid node. Lower case *x* is the great circle distance from the grid node to a proxy location. Provided there are 3 or more proxies within search distance *R* the grid node value is computed as the weighted average of the proxies centennial anomalies using weights defined by Eq. (A3).

CPD
7, 3349–3397, 2011

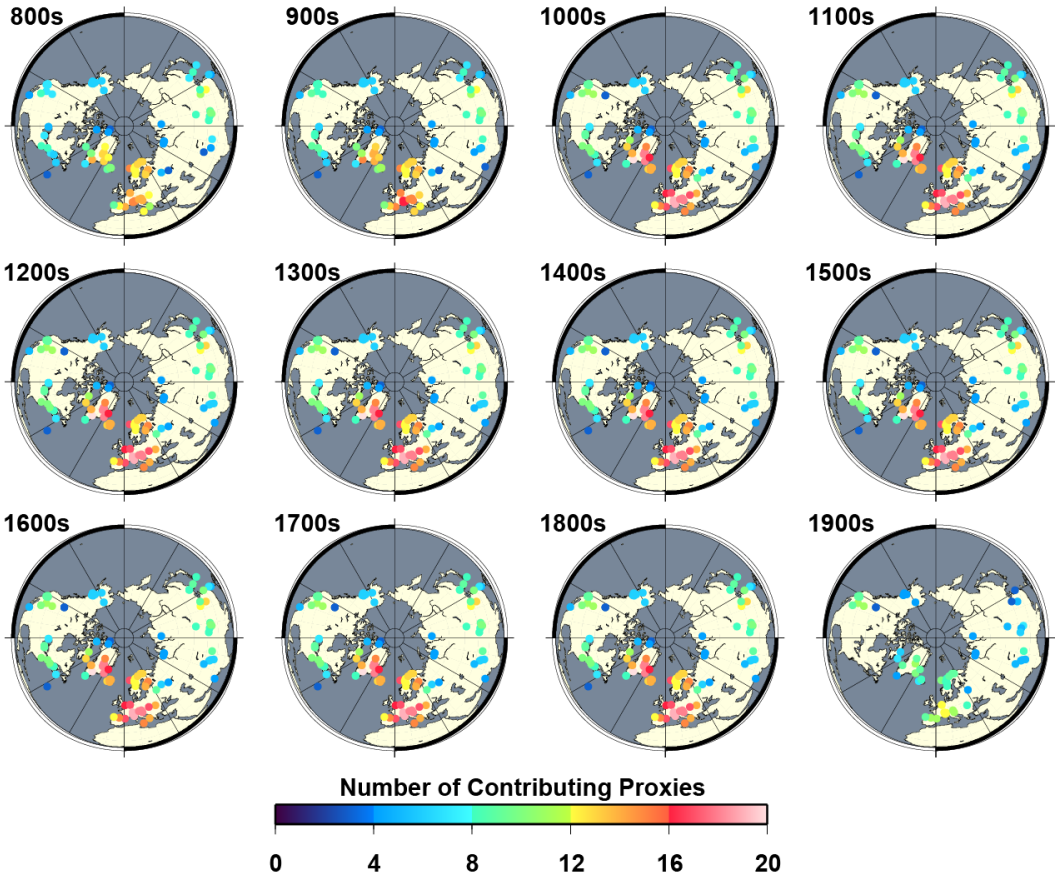

Fig. A6. Number of contributing proxies considered in each proxy-centered anisotropic weighted mean calculation where there are 3 or more neighbouring proxies found in the search radius.

CPD
7, 3349–3397, 2011

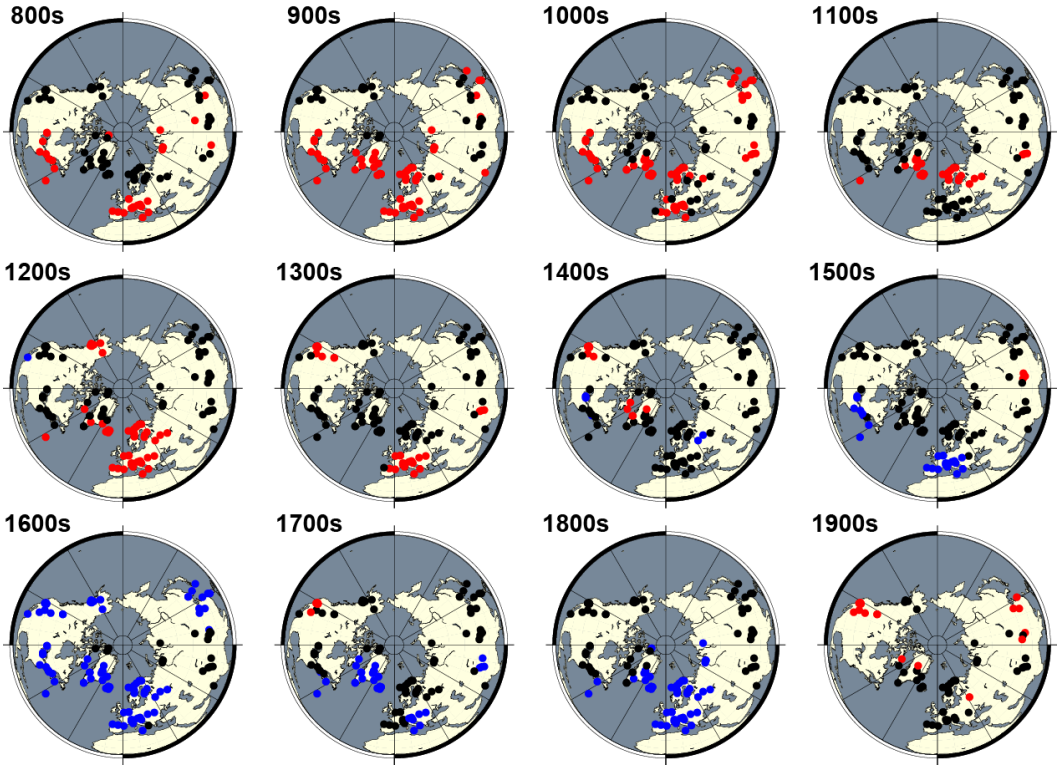

Fig. B1. Sign test of standardized centennial proxy anomalies. Red and blue dots indicate agreement within a search radius centered on each individual proxy location positive or negative, respectively. The search radii of the circles decrease linearly with latitude from 2000 km at the equator to 1000 km at the pole. Black dots indicate no significant agreement of the sign of anomalies.

CPD
7, 3349–3397, 2011

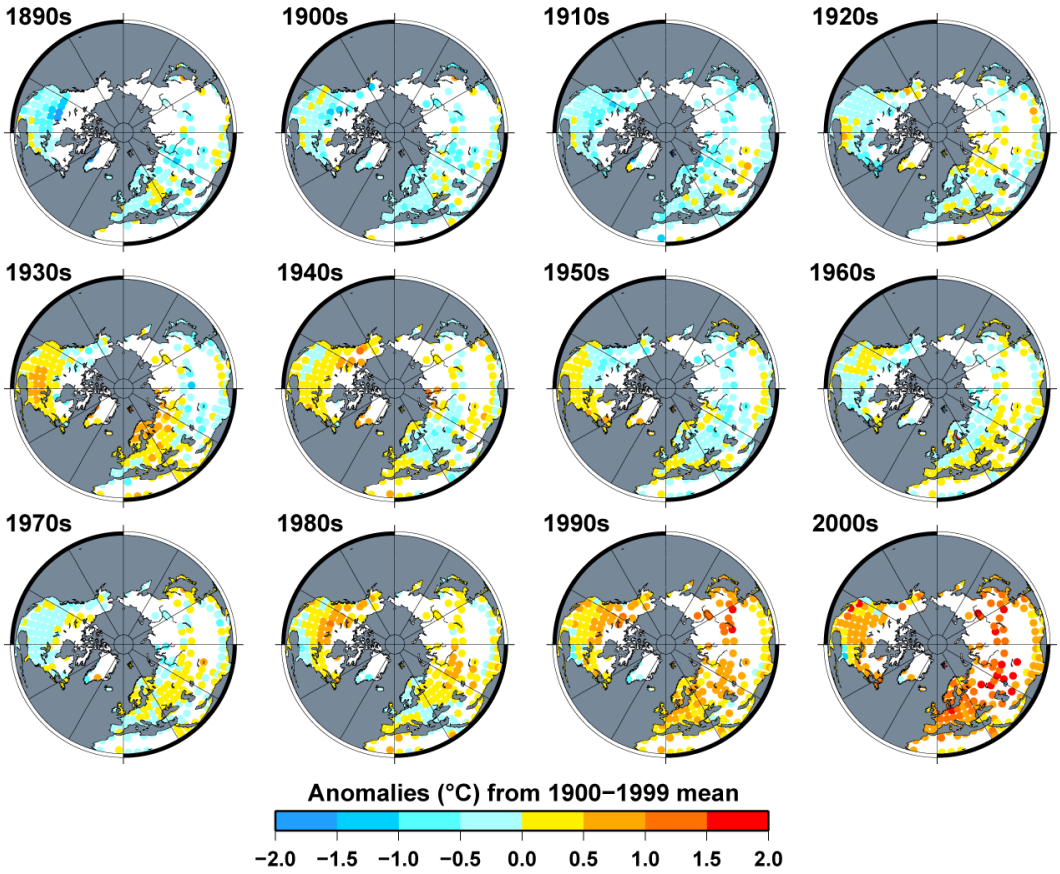

Fig. C1. Maps of decadal mean temperature anomalies (in ˚C) from the 1900–1999 mean, for all NH land grid boxes in the HadCRUT3 data set (Brohan et al., 2006) having at least 80 % complete monthly data. The labels 1890s and 1900s etc., denote the mean for the period 1890–1899 and 1900–1910 etc. Grid boxes over ocean areas are masked.

CPD
7, 3349–3397, 2011